JGR Oceans

RESEARCH ARTICLE
10.1029/2018JC014567

Key Points:
- The Pacific-derived Arctic water modifies structure of the Wandel Sea halocline
- During winter, northerly winds force the on-shelf Ekman transport of Pacific water (PW)
- During summer, southerly winds favor coastal upwelling forcing PW off-shelf

Variability of the Pacific-Derived Arctic Water Over the Southeastern Wandel Sea Shelf (Northeast Greenland) in 2015–2016

Igor A. Dmitrenko[1], Sergei A. Kirillov[1], Bert Rudels[2], David G. Babb[1], Paul G. Myers[3], Colin A. Stedmon[4], Jørgen Bendtsen[5], Jens K. Ehn[1], Leif Toudal Pedersen[6], Søren Rysgaard[1,7], and David G. Barber[1]

[1]Centre for Earth Observation Science, University of Manitoba, Winnipeg, Canada, [2]Finnish Meteorological Institute, Helsinki, Finland, [3]Department of Earth and Atmospheric Sciences, University of Alberta, Edmonton, Alberta, Canada, [4]National Institute for Aquatic Resources, Technical University of Denmark, Lyngby, Denmark, [5]ClimateLab, Copenhagen, Denmark, [6]National Space Institute, Technical University of Denmark, Lyngby, Denmark, [7]Arctic Research Centre, Aarhus University, Aarhus, Denmark

Abstract A portion of the freshwater transport through Fram Strait consists of low-salinity Pacific-derived Arctic water flowing southward along the east coast of Greenland. The pathways of this water are currently unclear. An Ice Tethered Profiler deployed over the southeastern Wandel Sea shelf (northeast Greenland) in May 2015 collected a profile every 3 hr for a year recording conductivity-temperature-depth (CTD) and Colored Dissolved Organic Matter (CDOM) fluorescence. This was accompanied by velocity observations. The CTD data revealed that the subsurface water (~15–85 m depth) characterized by high CDOM resembles the "cold Halostad" in the Canada Basin formed by the injection of Pacific water. A coastal branch of the Pacific water outflow from the Arctic Ocean supplies the Wandel Sea halostad, which shows a clear seasonal pattern. From July to October–November, the halostad is shallow, more saline, warmer, and with less CDOM. Conversely, from November to April, the halostad deepens, cools, freshens and CDOM increases, likely indicating a higher fraction of Pacific winter water. The CTD surveys, wind and current data, and numerical simulations show that the seasonal variation of wind over the continental slope likely controls seasonal changes of this intermediate water layer. Over northeast Greenland, winter winds have a northerly component from November to April, favoring Ekman transport of the Pacific-derived water to the Wandel Sea shelf. In contrast, the prevailing southerly summer winds result in retreat of the Pacific-derived water off the shelf. The landfast ice off-slope extension modifies wind-forcing disrupting seasonal patterns.

Plain Language Summary Arctic climate change is manifested in increased freshening of the surface seawater over recent decades due to increased precipitation, river runoff, and sea-ice and glacier melt. Over the coastal domains of northern Greenland, contributions from glacial melt are superimposed on the low-salinity surface water comprised by river runoff and low-salinity water of Pacific origin, while intermediate water is primarily of Atlantic origin. The glacier meltwater fraction can be significant, but its quantification requires differentiation from the Pacific water, the second largest source of the fresh water in the Arctic Ocean. To date, the Pacific-derived Arctic water component over the Greenland shelves remains poorly studied. The ice-tethered oceanographic mooring deployed over the southeastern Wandel Sea shelf (northeast Greenland) in May 2015 collected oceanographic data for a year. The obtained data and model simulations suggest that the Wandel Sea subsurface layer down to about 80 m depth is supplied by the coastal branch of the Pacific water outflow from the Arctic Ocean. This layer also shows a clear seasonal pattern likely indicating a higher fraction of the Pacific-derived water during winter. The seasonal variation of wind over the continental slope seems to control the Pacific water on-shelf inflow.

Correspondence to:
I. A. Dmitrenko,
igor.dmitrenko@umanitoba.ca

Citation:
Dmitrenko, I. A., Kirillov, S. A., Rudels, B., Babb, D. G., Myers, P. G., Stedmon, C. A., et al. (2019). Variability of the Pacific-derived Arctic water over the southeastern Wandel Sea shelf (northeast Greenland) in 2015–2016. *Journal of Geophysical Research: Oceans*, *124*, 349–373. https://doi.org/10.1029/2018JC014567

Received 21 SEP 2018
Accepted 16 DEC 2018
Accepted article online 19 DEC 2018
Published online 17 JAN 2019

1. Introduction

Low-salinity water from the Pacific significantly contributes to the Arctic Ocean freshwater budget (Serreze et al., 2006), which is also changing as a result of ongoing climate change (Holland et al., 2007; Rodell et al., 2018). In fact, Pacific Water (PW) is the second greatest source of freshwater to the Arctic Ocean (e.g., Carmack et al., 2016). PW enters the Arctic Ocean through the Bering Strait and spreads over the Arctic

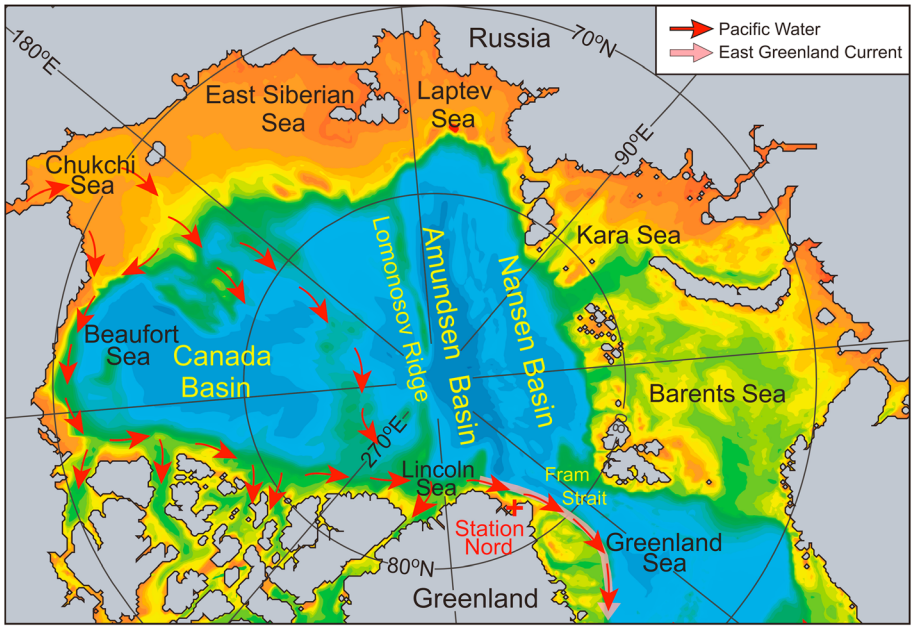

Figure 1. Schematic circulation of the Pacific Water (red arrows) in the Arctic Ocean and adjoining Greenland Sea following Jones (2001) and Woodgate (2013). The pink arrow indicates the east Greenland current. The red cross depicts the position of Station Nord in northeast Greenland.

Ocean along two major pathways, (i) a Transpolar branch that crosses the Arctic Ocean toward Fram Strait and (ii) an Alaskan branch that flows along the Beaufort Sea continental slope through the Canadian Archipelago and into Baffin Bay—Figure 1 (e.g., Aksenov et al., 2016; Hu & Myers, 2013; Watanabe, 2013). This has been confirmed by the detection of PW geochemical tracers in western Fram Strait, along northeast Greenland and in Baffin Bay (e.g., Alkire et al., 2010; Amon et al., 2003; Dodd et al., 2009, 2012; Falck, 2001; Jones et al., 1998, 2003). The Pacific-derived Arctic water comprises up to 20% of the freshwater inventory in the upper 300 m in western Fram Strait (Dodd et al., 2012) and dominates the freshwater inventory over the top 150 m in western Davis Strait (Alkire et al., 2010).

Climate change in the Arctic has increased freshwater content over the last several decades (Prowse et al., 2015). Recent increases in Arctic freshwater flux are primarily attributed to precipitation, river runoff, and sea-ice melt (Haine et al., 2015; Rabe et al., 2011). Over the coastal domains of eastern Greenland and in Baffin Bay, there are additional contributions from glacial melt (Bamber et al., 2018; Bendtsen et al., 2017; Castro de la Guardia et al., 2015) superimposed on Arctic freshwater flux that contains a variable PW fraction. Over the northwest Greenland shelf and coastal domains, the glacier meltwater fraction can also be significant (Bendtsen et al., 2017; Stedmon et al., 2015). The PW outflow complicates the direct estimates of the glacier meltwater fraction. The general contribution of the Pacific-derived Arctic water to the freshwater inventory remains poorly understood, partly due to seasonal and interannual variability of the PW inflow and outflow to/from the Arctic Ocean (e.g., de Steur et al., 2013; Dodd et al., 2012; Falck et al., 2005; Woodgate et al., 2005, 2012), but also because of the different pathways of PW in the Arctic Ocean (Aksenov et al., 2016; Hu & Myers, 2013). The coastal branch of the PW outflow through western Fram Strait is poorly resolved due to insufficient data coverage (e.g., Dmitrenko et al., 2017; Falck, 2001), however, numerical simulations indicate its presence (Aksenov et al., 2016; Hu & Myers, 2013) and PW is clearly observed downstream along the southeast coast of Greenland (e.g., Bacon et al., 2002; Jones et al., 2003; Sutherland et al., 2009; Sutherland & Pickart, 2008).

In the Canada Basin, the relatively fresh PW impacts the halocline structure, producing a double halocline layer with a low stratified Upper Halocline Water or "cold Halostad" formed by insertion of the cold winter PW that overlies Lower Halocline Water originating from the Eurasian Basin (McLaughlin et al., 2004; Shimada et al., 2005). The Arctic halocline water is also characterized by high concentrations of colored dissolved organic matter (CDOM), which can be traced using fluorometers (Guay et al., 1999). The CDOM within halocline waters from the Eurasian and Canada Basins (Low and Upper Halocline waters,

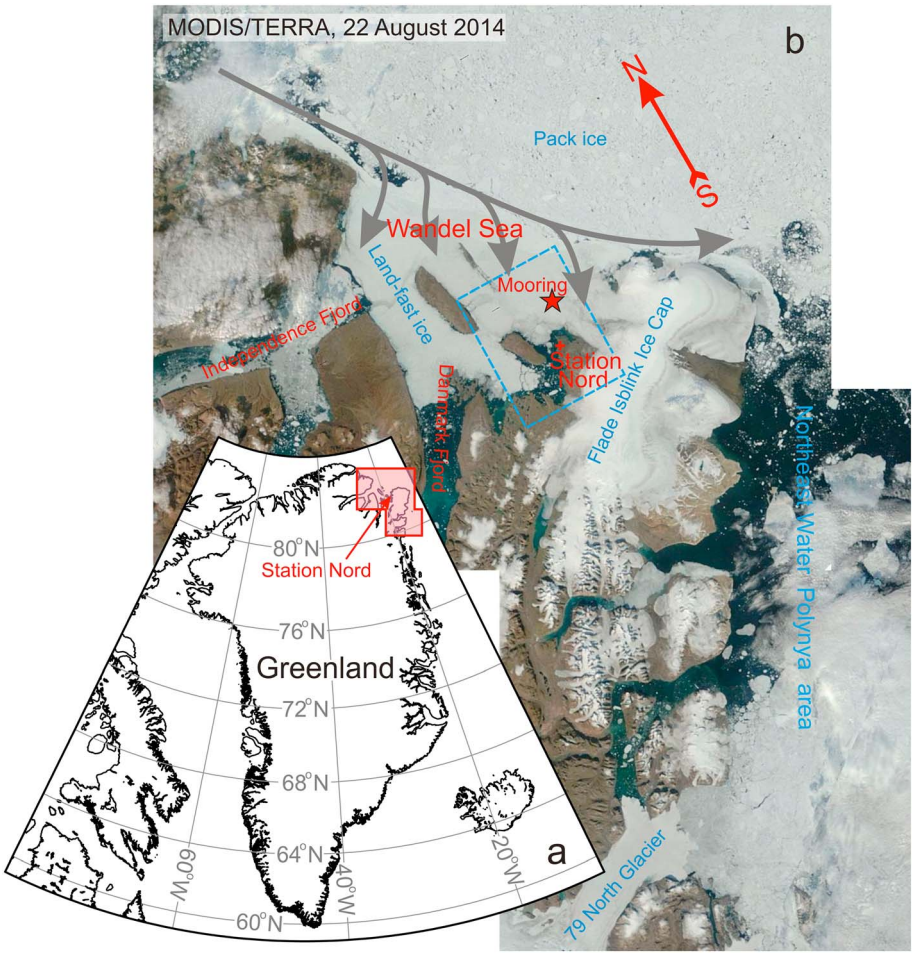

Figure 2. (a) SN on the Greenland map. The pink shading highlights the Wandel Sea region with the adjoining fjord system and Northeast Water Polynya area enlarged in b. (b) The MODIS/TERRA satellite image from 22 August 2014 taken over the SN/Northeast Water Polynya area. Red star indicates the mooring. Red cross depicts SN. The dashed blue rectangle indicates the 2015 study area shown in Figure 3. Gray arrows schematically depict coastal flow of the Pacific-derived Arctic water suggested by Dmitrenko et al. (2017). SN = Station Nord.

respectively) differ in origin. While the Atlantic-derived Eurasian halocline has a high content of terrestrial organic matter from Siberian rivers, the high CDOM content in the Pacific-derived Canada Basin halocline primarily originates from autochthonous production over the productive Chukchi shelf region (Stedmon et al., 2011). The low-salinity surface polar water including low-salinity water of Pacific origin and Pacific-derived halostad water leaving the Arctic Ocean through Fram Strait partly passes over the shelf area of the Wandel Sea. Following Dmitrenko et al. (2017), we use the physical and chemical characteristics mentioned above to detect and trace the Pacific-derived water fraction of the Arctic Ocean outflow on the northeast Greenland shelf (Figure 2). In the following we assign the Upper Halocline Water to the Pacific-derived Halostad and the Low Halocline Water to the Atlantic-derived Halocline.

A landfast ice-tethered mooring was deployed for 1 year from 15 May 2015 to 6 April 2016 over the southeast Wandel Sea outer shelf (Figure 2b). Mooring observations were complemented by three conductivity-temperature-depth (CTD) surveys over the southeast Wandel Sea shelf that were conducted from the landfast ice during April–May 2015 and April 2016 and in open water during August 2015 (Figures 3 and 4). The mooring was deployed as part of the first scientific expedition at the new Villum Research Station located at the Danish military outpost Station Nord. This project was conducted under the framework of the Arctic Science Partnership. Our objectives in this paper are to explore this data set along with results of PW passive tracers from a high-resolution numerical simulation to assess spatial and temporal variability of the Pacific-derived halostad. We hypothesize that variability is driven by lateral displacement of the PW

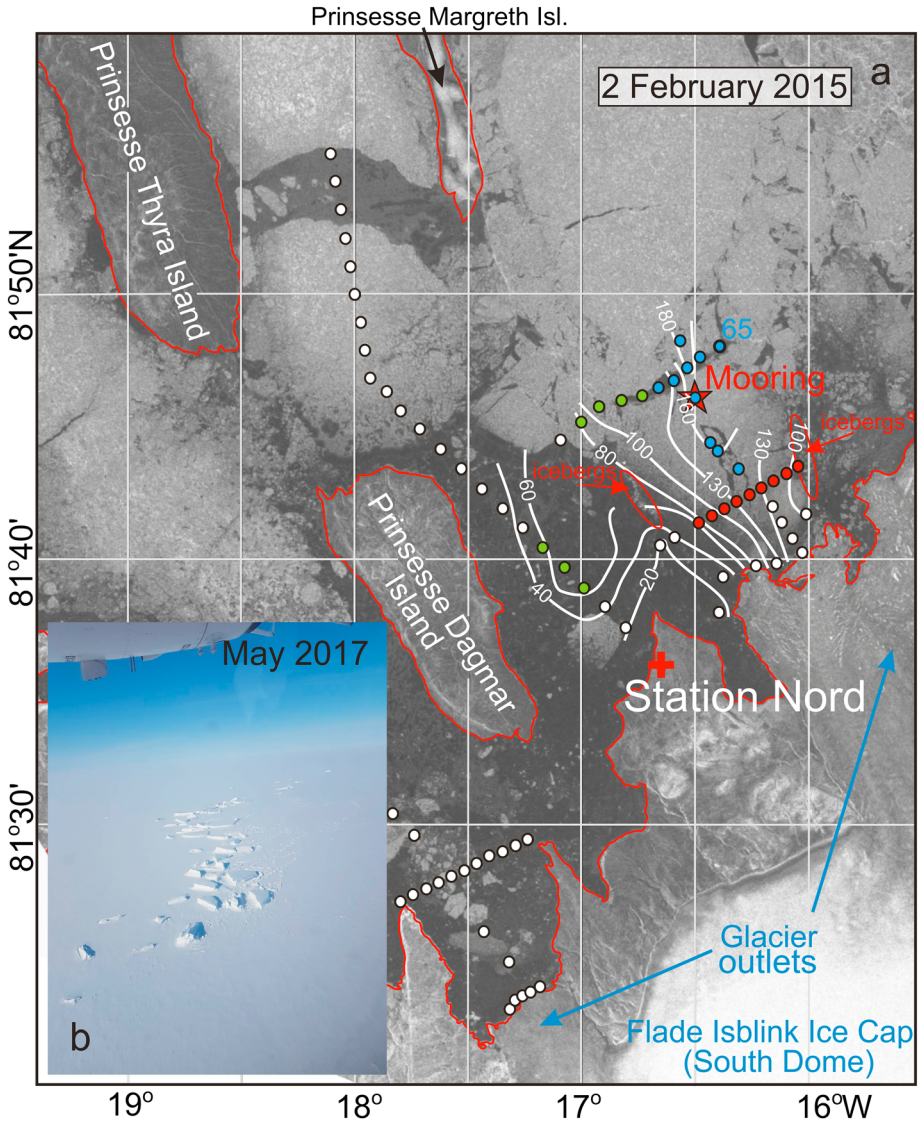

Figure 3. (a) The Sentinel-1 C-band SAR image taken over the eastern Wandel Sea shelf on 2 February 2015 with the CTD stations and mooring overlaid. Red star depicts the mooring. Colored circles identify CTD stations used for this research with CTDs showing winter (blue), summer (red), and transitional (green) modes of the Pacific-derived halostad as depicted with similar colors in Figure 5 and explained in section 3.1. White circles identify CTD stations not used for this research. Depth shown by white contour lines. Blue arrows indicate the northern outlet glaciers of the Flade Isblink ice cap. The lighter areas indicate the multiyear landfast ice (~2 to >4 m thick). Red elapses highlight areas of icebergs, which are hardly recognizable on the SAR imagery. (b) Aerial photo taken from the aircraft before landing at Station Nord on May 2017 shows icebergs grounded on the marginal lateral moraine flanking the southwestern rim of the glacier trough; credits: I. Dmitrenko. CTD = conductivity-temperature-depth.

bearing coastal jet, which is suggested to flow along the shelfbreak of northeast Greenland (Figure 2b). Here we focus on the halostad observed in the 15–85 m depth range, and more specifically the cooler halostad located at 55–85 m depth, which shows the most significant seasonal and spatial variability.

The Wandel Sea represents a glacial inlet that is composed of several fjords that open to the northeast Greenland continental slope (Figure 2). It is covered by landfast sea ice all year, with open water only forming in the interior of the fjords during August and September (Figure 2b). Note that in August 2016 the multiyear landfast ice bridge over the Wandel Sea outer shelf became unstable, and a sizeable portion of the ice cover east of Prinsesse Margreth Island collapsed in August 2017. The eastern landfast ice edge (Figure 2b) roughly delineates the Wandel Sea continental shelf break, which is where a coastal polynya opens in response to southerly winds. The Wandel Sea shelf bottom topography is poorly known.

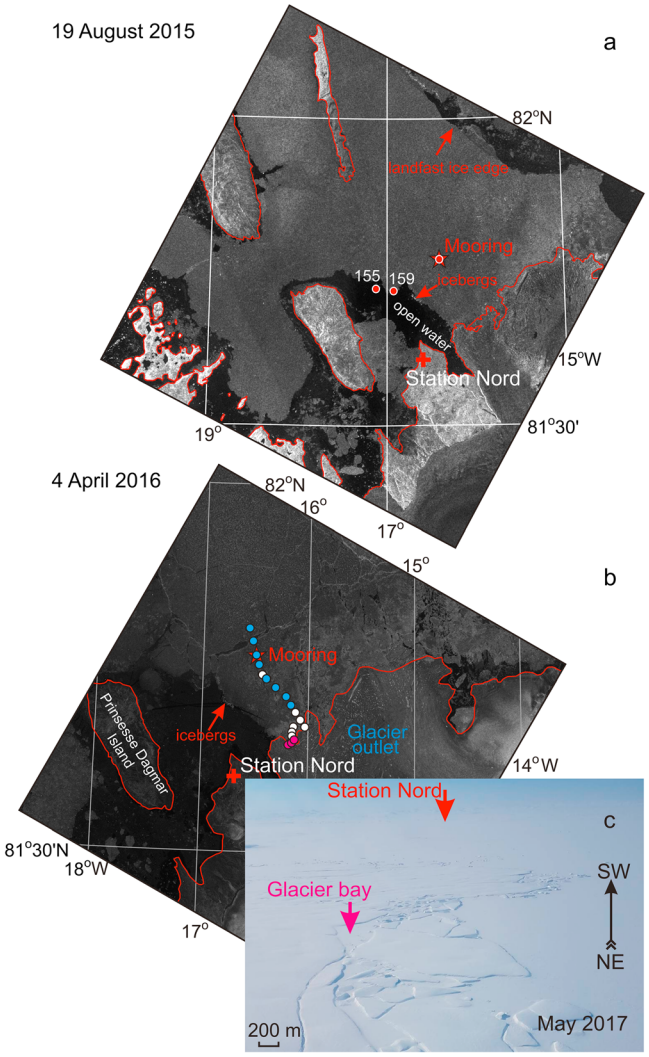

Figure 4. The Sentinel-1 C-band SAR images from (a) 19 August 2015 and (b) 4 April 2016 with the CTD stations and mooring overlaid. Colored circles identify CTD stations used for this research with CTDs showing winter (blue), summer (red), and glacier (purple) modes of the Pacific-derived halostad as depicted with similar colors in Figure 5. (a) The dark areas indicate the open water. (c) Aerial photo taken over the tidewater glacier outlet in May 2017; purple arrow highlights the glacier bay where CTDs occupied in April 2016 (credits: I. Dmitrenko). The spatial scale at left bottom is approximate. CTD = conductivity-temperature-depth.

The most comprehensive bathymetry data set compiled by Nørgaard-Pedersen et al. (2016) revealed a glacier trough in front of the tidewater glacier terminus of the Flade Isblink ice cap (Figures 2b and 3a), which is an isolated ice cap with a surface area of 5,000 km^2 and maximum thickness of 600 m (e.g., Palmer et al., 2010; Rinne et al., 2011). The glacial trough is open to the continental slope with depth varying from ~130 m at the tidewater glacier terminus to about 180 m at the mooring location (Figure 3). The trough allows Atlantic-derived Arctic water with temperatures >0 °C to flow into the Wandel Sea shelf at depths greater than 140 m (Dmitrenko et al., 2017; Limoges et al., 2018). The glacier trough is flanked on both sides by numerous icebergs (Figure 3b) that are grounded on the ~80 m deep marginal lateral moraine, which reduces lateral exchange with ambient water from the continental slope (Figures 3a and 4). The glacier trough area is separated laterally from the midshelf by ~20–30 m deep shoals preventing the halostad from extending over the entire Wandel Sea shelf (Figure 3a).

Prior to the field programs in 2015–2016, there were no oceanographic data collected over the Wandel Sea shelf. In contrast, the more easily accessible downstream Northeast Water Polynya (NEW) area (Figure 2b) was well explored during the polynya-focused international programs in 1992–1993 (e.g., Bignami & Hopkins, 1997; Budéus et al., 1997). Using this data set, Falck (2001) was first to suggest a Pacific origin for the NEW on-shelf halostad. Following Falck (2001) and using recent CTD observations, Dmitrenko et al. (2017) suggested that Pacific-derived Arctic water flowing along the upper Wandel Sea continental slope (Figure 2b) was the source of the cold halostad in the Wandel Sea. Using a 3-week time series from the landfast ice-tethered mooring deployed at the front of the northern outlet of the Flade Isblink ice cap in April 2015, Kirillov et al. (2017) reported on storm-induced downwelling with onshore water transport in the surface (0–40 m) layer and compensating offshore flow at intermediate depths. For the Wandel Sea region adjacent to the tidewater glacier terminus, both Dmitrenko et al. (2017) and Kirillov et al. (2017) reported on water properties modified by the ocean-glacier interactions for depths exceeding 90–100 m. During summer (August 2015), the glacier marine melt also affects the surface fresh water flux (Bendtsen et al., 2017). Here we build on results by Dmitrenko et al. (2017) on the Pacific-derived halostad layer over the Wandel Sea outer shelf extending our analyzing on the year-long CTD and velocity mooring time series and CTD surveys conducted in August 2015 and May 2016. Our main goal is to explain seasonal variability of the halostad in response to wind forcing over the Wandel Sea continental slope.

2. Data and Methods

The landfast ice-tethered oceanographic mooring was deployed over the southeast Wandel Sea outer shelf at 81.768°N, 16.502°W from 15 May 2015 to 6 April 2016. The mooring was located ~15 km from Station Nord, ~18–20 km from the landfast ice edge, and ~14 km from the tidewater glacier terminus at 178 m depth along the glacial trough that opens to the continental slope (Figures 2b and 3). The mooring was deployed through a refrozen melt pond on 2.6 m thick multiyear landfast ice. The mooring setup consisted of two Workhorse 300 kHz Acoustic Doppler current profilers (ADCPs) placed at 3.3 m (down-looking) and at 174 m (up-looking), two SBE-37 CT sensors by Sea-Bird Electronics placed at 3.5 and 166 m, and an Ice Tethered Profiler (ITP) by McLane Research Laboratory preprogramed to cast every 3 hr in the depth range from 4.4 to ~150 m. The ITP was equipped with a CTD sensor 41CP by Sea-Bird Electronics and Wetlabs ECO sensor for

measuring backscatter intensity, chlorophyll fluorescence, and CDOM fluorescence for EX/EM = 370/460 nm. CTD and optical data were recorded approximately every 0.3 and 1.5 m, respectively. According to manufacturer specifications, the CTD sensor 41CP accuracy is ±0.002 °C, ±0.002 salinity units, and ± 2 dbar with a typical stability of 0.0002 °C, 0.001 and 0.8 dbar per year, respectively. The CDOM fluorometer was calibrated to quinine sulfate and had a sensitivity of 0.28 parts per billion (ppb). The high-quality ITP CTD record was confirmed by observed agreement between the upper/lowermost ITP measurements at 4.4/150 m depth and the upper and lower SBE-37 s at 3.5/160 m depth, respectively. All sensors were calibrated by manufacturers prior to the expedition.

The velocity data were obtained at 2 m depth intervals, with a 30 min ensemble time interval and 30 pings per ensemble. For the downward-looking ADCP the first measured bin was located at 8 m depth (i.e., about 5 m below the ice), and ADCP measured the water layer down to 60–80 m depth. This ADCP stopped working on 26 December 2015, and there was a data gap from 7 July to 7 August 2015 when the ADCP transducer was blocked by a platelet ice layer (for more details see Kirillov et al., 2018). For the upward-looking ADCP the first bin was at l70 m depth, and the ADCP sampled the water column up to 90–110 m depth. The RDI ADCPs precision and resolution are ±0.5% and ±0.1 cm/s, respectively. The compass accuracy was estimated to ±8° due to the small horizontal component of the Earth's magnetic field in the Wandel Sea (for more details see Kirillov et al., 2018). The measured current direction was corrected for the local magnetic deviation (~18°W).

Mooring data were complemented by synoptic CTD surveys in April–May and August 2015 and April 2016. Between 17 April and 15 May 2015, 86 CTD profiles were collected from the landfast sea ice (1.0 to 3.5 m thick) on the Wandel Sea shelf (Dmitrenko et al., 2017, and Figure 3a). For this study we used only 26 of these profiles, that is, those (i) taken east of the 17°30′W, (ii) exceeding 60 m depth, and (iii) located well away from the tidewater glacier terminus (Figures 3a and 5a–5c). During the summer survey (10–21 August 2015), 115 CTD casts were collected over the ice-free area using inflatable boats (Bendtsen et al., 2017). Within this study we only use CTDs from Stations 155 and 159 that were collected on 21 August along the shore side of the landfast ice edge (Figures 4a, 5d, and 5e). These two stations were taken over the southwestern rim of the glacier trough with depth exceeding 60 m, and close (~8–10 km) to the mooring position. During 4–13 April 2016, 31 CTD profiles were taken from the landfast ice primarily along the oceanographic section following the glacier trough and adjacent to the tidewater glacier terminus. Here we use eight profiles from the glacier trough and three profiles taken at the semi-isolated glacier bay of ~2 km in diameter surrounded by the tidewater glacier terminus (Figures 4b, 5f, and 5g). The glacier profiles were selected to assess how ocean-glacier interactions influence the Pacific-derived halostad. The CTD observations were carried out with a SBE-19plus CTD that was calibrated by the manufacturer prior to the expedition and was accurate to ±0.005 °C and ±0.0005 S/m.

Ice conditions over the Wandel Sea shelf, the adjoining fjords, and the Greenland Sea continental slope were monitored by Moderate Resolution Imaging Spectroradiometer (Figure 2b) and Sentinel-1 C-band SAR (C-Band Synthetic Aperture Radar) satellite imagery, acquired daily by the Danish Meteorological Institute (http://ocean.dmi.dk/arctic/nord.uk.php). In general, open water, newly formed sea-ice, ice ridges, multiyear and first-year landfast sea ice, refrozen leads, large icebergs, and glacier terminations are distinguishable in SAR imagery. Sea ice thickness was measured manually at each CTD station with an ice thickness tape. A time series of the 10 m wind over the Wandel sea continental slope (82°N, 15°W) was obtained from the National Centers for Environmental Prediction (NCEP)—(Kalnay et al., 1996). NCEP winds have been shown to agree with local in situ winds from the Station Nord weather station (Kirillov et al., 2017).

The passive tracer analysis was carried out in a simulation of the Nucleus for European Modeling of the Ocean (NEMO) version 3.4 (Madec & the NEMO team: NEMO ocean engine, 2008). The Arctic and the Northern Hemisphere Atlantic configuration, run at 1/12°, was used. The horizontal resolution over the western Arctic is ~4–5 km. The sea ice module used here is the Louvain la-Neuve Ice Model Version 2 with an elastic-viscous-plastic rheology (Hunke & Dukowicz, 1997), including both thermodynamic and dynamic components (Fichefet & Maqueda, 1997). The model domain covers the Arctic and the Northern Hemisphere Atlantic with two open boundaries, one close to Bering Strait in the Pacific Ocean and the other one at 20°S across the Atlantic Ocean. Open boundary conditions (temperature, salinity, and horizontal ocean velocities) are derived from the monthly Global Ocean Reanalysis and Simulations produced by Mercator

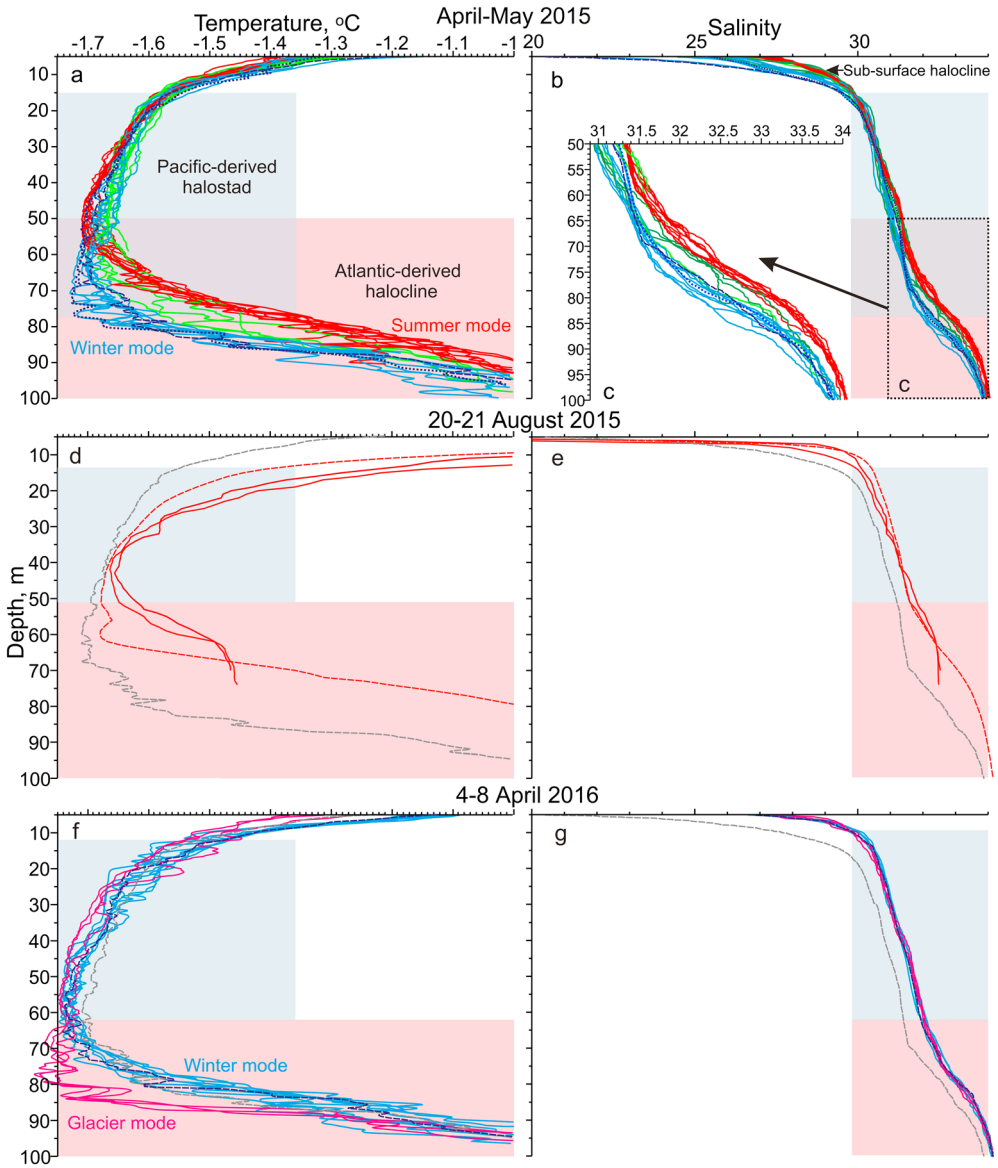

Figure 5. Vertical distribution of (a, d, and f) temperature (°C) and (b, c, e, and g) salinity over the southeastern Wandel Sea shelf (>60 m depth) in (a, b, c) April–May 2015, (d, e) 20–21 August 2015, and (f, g) 4–8 April 2016 through the upper 100-m layer. Red, blue, green, and purple lines indicate the summer, winter, transitional, and glacier modes, respectively. Dashed lines show moored Ice Tethered Profiler profiles. Dotted lines in (a) and (b) are from station #65 (see Figure 3). Gray dashed lines in (d)–(g) are the Ice Tethered Profiler profiles taken in 15 May 2015 as in (a)–(c). Blue and pink shading highlights the Pacific-derived halostad and Atlantic-derived halocline, respectively.

Ocean (Masina et al., 2017). The simulation was integrated from 1 January 2002 to 31 December 2016, driven with high temporal (hourly) and spatial resolution (33 km) atmospheric forcing data provided by Canadian Meteorological Centre Global Deterministic Prediction System ReForecasts data set (Smith et al., 2014). There is no salinity restoring. Further details, as well as model evaluation, can be found in Hu et al. (2018) and Courtois et al. (2017). The passive tracer is introduced into the model at the Bering Strait uniformly with depth, starting from the beginning of the model experiment on 1 January 2002. The amount of tracer input is proportional to the volume flux in each grid cell at the Bering Strait. Thus, the tracer flux replicated the seasonal and interannual variability of the Bering Strait inflow. For the Wandel Sea continental slope and outer shelf fields are presented as depth integrated through the 20–85 m depth layer that is roughly associated with the Pacific-derived halostad.

3. Results

3.1. CTD Survey in April–May 2015

The water mass description for the southeast Wandel Sea shelf made by Dmitrenko et al. (2017) based on CTD profiles occupied in April–May 2015 assigned a halostad layer from about 15 to 65 m depth to Pacific-derived water. This interpretation is based on similarities between the Wandel Sea halostad and the cold halostad of Pacific origin identified in the Canada Basin by Shimada et al. (2005). The Pacific-derived halostad in the Wandel Sea is characterized by weak vertical salinity difference (salinity 30 to 31.2–31.5) and water near the freezing point (Dmitrenko et al., 2017). At the top of the Pacific-derived halostad, the subsurface halocline layer with a strong vertical salinity gradient (salinity 1 m^{-1}) separates the halostad from the relatively fresh (salinity of 16–21, not shown) surface layer that forms locally from snow and sea-ice meltwater (Kirillov et al., 2018) and freshwater from the glacial runoff (Bendtsen et al., 2017). Below the Pacific-derived halostad, the Atlantic-derived halocline can be found with salinities between 31.5 and 34. The Atlantic-derived thermocline is characterized by temperatures steadily increasing with depth up to >0 °C in the Atlantic layer at depths exceeding 140 m (Dmitrenko et al., 2017). In Figure 5 the Pacific-derived halostad and Atlantic-derived halocline are highlighted with blue and pink shading, respectively.

A more detailed view on the Wandel Sea halostad in April–May 2015 reveals that over the southeast shelf area covered with CTD data and limited to about 25 × 25 km (Figure 3), the halostad shows significant spatial variability with depths of its lower boundary varying from 55 to 77 m (overlapping between blue and pink shading in Figures 5a and 5b). In fact, the halostad shows two different modes that results in a splitting of the Atlantic-derived halocline for both temperature and salinity profiles through the 50–100 m depth range (Figures 5a and 5c). On average, the deep mode of the halostad is ~12–15 m deeper than the shallow mode (blue and red profiles in Figures 5a and 5b, respectively). The depths of the halocline change accordingly (Figures 5a and 5b). At the base of the deep halostad mode from 65 to 77 m depth, water is cooler by ~0.15 °C (Figure 5a) and fresher by ~0.7 (Figure 5c) than the shallow mode.

The spatial analysis assesses the main patterns of the deep and shallow halostad and relates them to their geographical location on the southeast Wandel Sea shelf area covered with CTD data. A deep halostad with a base comprised by cooler and fresher water occupies the deeper glacier trough and extends over its eastern flank open to the Wandel Sea continental slope (blue dots in Figure 3). The minimum water temperature of −1.73 °C at the base of the halostad at 70 m depth was observed at station 65, that is, the station closest to the Wandel Sea continental slope (Figures 3 and 5a). In contrast, a shallow halostad is recorded in the middle of the glacial trough and its flanks (red dots in Figure 3). Note that CTDs occupied at proximity to the tidewater glacier terminus were excluded from this analysis (Figure 3) due to the ocean-glacier modifications imposed at the base of the halostad (Dmitrenko et al., 2017). However, we will address this point below in section 3.3 where we discuss CTD data from April 2016. All other stations from this CTD survey involved in our analysis represent the transition from a deep to shallow halostad. They occupy the western flank of the glacier trough open to the Wandel Sea midshelf area (green dots in Figure 3 and green lines in Figures 5a–5c).

Overall, over a rather limited area in the southeast Wandel Sea shelf, we detect two different halostad modes clearly showing spatial regularities. In the following we refer to a deep (cooler and fresher) mode as the "winter" mode, and a shallow (warmer and saltier) mode as the "summer" mode. This attribution is primarily based on the thermohaline properties at the base of the halostad showing spatial regularities over the southeast Wandel Sea shelf. In the following, however, we will link these spatial features to seasonal variability.

3.2. CTD Survey in August 2015

Two CTD casts used for this study were taken on 21 August 2015 from the open water near the interior landfast ice edge over the western flank of the glacier trough (Figure 4a). In terms of the halostad, these CTD casts closely resemble the summer mode of April–May 2015 (Figures 5a–5e). The base of the halostad at ~40 m depth (~10–15 m shallower comparing to April–May) shows a minimum temperature of −1.66 °C at a salinity of 31.3, and this is ~0.02 °C warmer and 0.25 saltier comparing to April–May. At its upper boundary (15 m depth), the August halostad was found to be ~0.3 °C warmer and 0.25 saltier, that is, the same salinity anomaly as observed at the lower boundary. Thus, seasonal freshening expected through the upper water layer due to fresh water flux from snow, sea-ice, and glacier melt was not observed. The most

significant changes, however, occurred over the central part of the glacier trough (dashed lines in Figures 5d and 5e). Based on moored CTD data, the halostad has been shallowed from 68 to ~50 m depth. The associated changes in temperature and salinity at 50 m depth are recorded to ~0.02 °C and 0.3, respectively, showing similar tendencies as over the western flank of the glacier trough. At 15 m depth, the glacier trough halostad was warmer and saltier by ~0.13 °C and 1.0, respectively, relative to April–May.

Overall, the general assessment of the halostad variability from April–May to August is that the summer mode expanded from the midtrough to the western flank and mooring position substituting the transitional and winter mode. However, the increase in salinity through the upper halostad at the mooring location (~1) is unlikely to be explained by alternating from winter to summer mode. For April–May 2015 at 15 m depth the summer mode salinity exceeds salinity at mooring position only by ~0.3.

3.3. CTD Survey in April 2016

CTD profiles taken on 4–8 April 2016 along the glacier trough show only the winter mode of the halostad (Figures 4b, 5f, and 5g). In April 2016, no CTD stations were taken over the western flank of the glacier trough, and the summer mode was likely therefore not sampled. The halostad was recorded ~7 m shallower, 0.4 °C cooler, and 0.8 saltier comparing to April–May 2015. Thus, if the seasonal cycle occurs through the Pacific-derived halostad, then it is not closed due to salt influx observed from 2015 to 2016. This tendency is also evident from CTD profiles carried out in August 2015 (Figures 5d and 5e). As of April–May 2015, the minimal temperature (−1.73 °C) was recorded at the base of the halostad at ~60 m depth (Figure 5f).

CTD profiles occupied in April 2016 at the semi-isolated glacier bay surrounded by the tidewater glacier terminus (purple dots in Figure 4b) show the potential of the tidewater outlet glacier for modifying water properties through the Atlantic-derived halocline. These three CTD profiles, grouped into the halostad glacier mode, show exceptionally low water temperatures down to −1.79 °C through 63–85 m depth (purple lines in Figure 5f). As a result, the upper 20-m portion of the Atlantic-derived halocline does not show a temperature increase with depth, as typical for profiles comprising the upper part of the halocline (Figures 5a–5e).

Based only on temperature profiles, one may suggest that the purple profiles in Figure 5f represent the winter halostad deepened down to ~85 m. However, the corresponding salinity profiles through this depth range are not modified accordingly and look similar to those taken over the glacier trough ~5–10 km from the tidewater glacier terminus (Figure 5g). Thus, the relatively cold temperatures can only be explained if the upper portion of the halocline was thermally modified without freshening involved, that is, cooled by glacier ice.

Water cools when it comes in contact with glacier ice that is colder than the in situ freezing point of seawater, and if the water temperature is below the freezing point of the glacier ice then this cooling is not associated with freshening. The glacier mode profiles in Figure 5f represent an example of the glacier-ocean thermal interaction without significant glacier melt contribution. Note, however, that all CTD profiles taken from the landfast ice at the vicinity of the tidewater glacier terminus show cooler and fresher water below 100 m depth compared to ambient profiles taken well away from the glacier terminus (not shown). Moreover, the mooring optical data of CDOM fluorescence presented below (section 3.4.2) allow to differentiate the Pacific-derived halostad from the glacier-modified halocline.

3.4. Mooring Data From May 2015 to April 2016

3.4.1. ADCP Velocity Data

For this research we use velocity data from 8, 50, and 160 m depth. The velocity time series at 8 m is from the uppermost down-looking ADCP bin and indicates the under-ice water dynamics. The 50 m depth velocities are intended to describe the halostad water dynamics and derived from the deepest bin of the ice-tethered downward-looking ADCP. During winter the profiling range was significantly reduced due to insufficient scattering in the water column, and the base of the halostad at ~50 to 75 m depth is unresolved with velocity data. ADCP data at 160 m, well below the depth of the 0° isotherm separating the Atlantic Water layer from the upper layers (~140 m depth, Dmitrenko et al., 2017), describe the Atlantic water layer dynamics.

Figure 6 shows a progressive vector diagram based on the 24-hr mean ADCP velocity time series for each selected depth. From the mooring deployment on 16 May 2015 (Julian day JD136) to 5 August (JD217), the sub-ice water layer shows insignificant water transport (Figure 6a) with a mean speed of 0.3 ± 1.4 cm/s to the east (90°). Following JD217 and until 16 October (JD289), a northeast flow aligned to ~70° was observed with a mean velocity of 4.0 ± 3.1 cm/s. During this time the hypothetical water parcel would

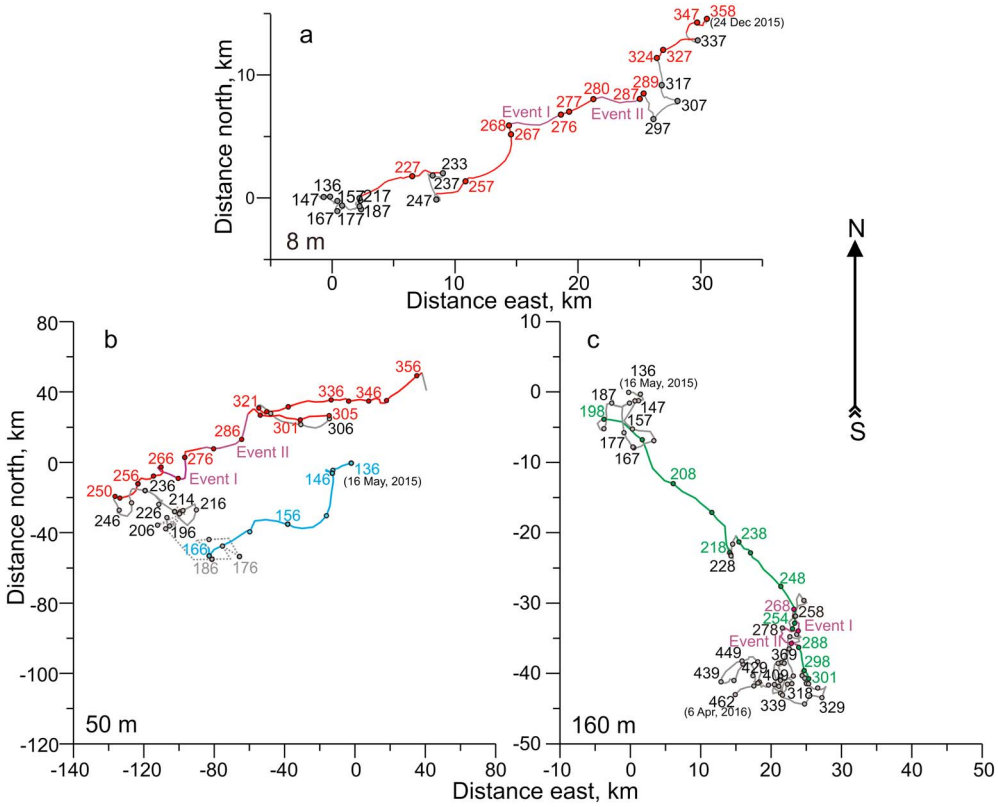

Figure 6. Progressive vector diagram for the ADCP 2-m binned current record at (a) 8, (b) 50, and (c) 160 m depth. Blue and green lines highlight on-shelf inflow (b) across the shelfbreak and (c) along the submarine glacier valley, respectively. (a, b) Red line highlights shelf outflow. Purple lines indicate storm events also depicted in Figures 7 and 9. Dashed line indicates no reliable data. Numbers show the Julian days.

have been transported ~25 km from the source region located over the western flank of the glacier trough. Based on satellite imagery, the first-year landfast ice was rapidly retreating from this area since 16 August 2015 (not shown), and on 19 August the region was already ice free (Figure 4a). The northeastward shelf outflow was interrupted from 21 August to 7 September (JD233–250) and modified during events I (25 September to 3 October, JD268–276) and II (7–16 October, JD280–289)—Figure 6a. After 20 November (JD324), the northeast water transport was restored and dominated until the end of the ADCP record (24 December 2015, JD358).

In contrast to the sub-ice water layer, the halostad at 50 m depth shows an on-shelf flow aligned to 237° at 3.7 ± 2.8 cm/s from the day of deployment to 15 June (JD136–JD166)—Figure 6b. During this inflow event, the hypothetical water parcel can potentially be transported ~100 km from the area located over the Wandel Sea continental slope, across the Wandel Sea outer shelf, to the mooring location (note that the mooring was deployed ~20 km from the Wandel Sea shelfbreak). Afterward, the down-looking ADCP transducer was blocked by the platelet ice layer until 2 August (JD214), and no significant dynamics was recorded until 7 September (JD250)—Figure 6b. Since that time, a consistent shelf outflow of ~2.0 ± 1.8 cm/s aligned to 68° was recorded almost until the end of the record on 24 December 2015. In fact, this flow was in the exact opposite direction to the shelf inflow observed for JD136–166 (Figure 6b). This outflow, however, was reversed for 1–17 November (JD305–321) and modified during events I and II, similarly to the 8 m depth level (Figures 6a and 6b). However, the direction was more aligned to the south during the initial phase of disturbance that seems to be in accordance with the Ekman spiral responding to wind forcing.

For the Atlantic water layer at 160 m depth, the period after deployment to 17 July (JD198) is characterized by weak water dynamics without considerable water transport, similar to the sub-ice water layer. Afterward, an on-shelf inflow aligned to 138° at 0.8 ± 0.6 cm/s was observed until 11 September (JD254)—Figure 6c. This flow direction corresponds to the orientation of the glacier trough open to the Wandel Sea

continental slope that is ~55 km northeast of the mooring position (Figures 2b and 3a). From JD198 to JD254, the hypothetical water parcel can be transported along the glacier trough by ~40 km (Figure 6c), and on the mid of September 2015 the water sampled by the mooring can originate from the Wandel Sea continental slope. The along-trough water inflow was interrupted from 12 September to 15 October (JD255–288), particularly by events I and II, but then continued to 164° with a speed of 0.6 ± 0.4 cm/s to 28 October (JD301). Afterward, until mooring recovery on 6 April 2016 (JD462), no considerable water flow was recorded (Figure 6c).

3.4.2. ITP CTD and CDOM Data

Figures 7b–7d show the year-long measurements of temperature, salinity, and CDOM fluorescence, respectively, from the landfast ice-tethered ITP profiler. Before going into details, we point out that the entire ITP record shows the halostad enriched with CDOM, as was reported by Dmitrenko et al. (2017) for the short-term mooring deployed at the front of tidewater glacier terminus in April 2015. The CDOM temporal variability reflects the structure of the halostad and underlying halocline from ~15 to 90 m depth (Figure 7). The subsurface melt water layer with salinity <25 and Atlantic water layer with salinity >34.5 below 130–140 m depth have a lower CDOM content (<80 ppb).

Based on tendencies of CTD and CDOM fluorescence, we conventionally subdivided the entire mooring record to the (i) relatively stable period to the end of June (~JD180), (ii) transition period from the end of June to the end of October (~JD300), (iii) relaxation period from the end of October to February (~JD420), and again (iv) the relatively stable period from the end of February to the end of record in April 2016—Figure 7 bottom. Below we focus on each period, also putting them in a context of water dynamics (Figures 6 and 7a) and the regional CTD surveys carried out in April–May and August 2015, and April 2016 (Figure 5).

During the stable period in May–June 2015, no significant variability was observed, while the boundary between the halostad and halocline traced by the 32.5 isohaline was slightly shallowed by ~8 m (Figures 7b and 7c). It was accompanied by reduction of CDOM fluorescence at the lower and upper boundaries of the halostad from ~107–108 to 105 ppb, and through the halocline from 107 to 90 ppb (Figure 7d). The under-ice water layer at 5–10 m depth and Atlantic water layer below 140 m depth remained relatively stable (Figures 7b–7d). Note that during this period the on-shelf inflow was observed in the halostad (Figure 7a).

The transition period is characterized by the northeastward shelf outflow for the sub-ice (8 m depth) and halostad (50 m depth) layers and inflow for the Atlantic water (160 m) along the glacier trough (Figures 6 and 7a). This was accompanied by significant modifications through the entire water column (Figures 7b–7d). The under-ice 10-m thick water layer shows warming (up to ~2.5 °C) and freshening (down to 17–20) attributed first to the drainage of snow meltwater through the landfast ice (JD196–216) and then to a pulse of warm meltwater advected from the ice-free area generated over the western flank of the glacier trough to southwest of the mooring location (JD226–247, Figure 4)—Kirillov et al. (2018). This is confirmed by the velocity time series at 8 m depth showing consistent northeastward flow starting JD218 (Figures 6a and 7a). For the deeper layer below 10 m depth, the halostad, halocline, and underlying Atlantic water layer were elevated up to 20 m as follows. The temperature and salinity time series show gradual shallowing of the halostad lower boundary from ~65–70 m depth in May–June 2015 to ~35–40 m depth to the mid-September (Figures 7b and 7c). During this time, the salinity at 65 m depth increased from ~31.50 to 33.15 (Figure 7c) accompanied by warming from approximately −1.7 °C to −1.45 °C (Figure 7b), while at 35 m depth salinity increased from 30.8 to 31.6 as temperatures remained constant. At the top of the halostad (~15 m depth) salinity increased from 30 to 30.8 and the temperature increased by ~0.2 °C. The shallowing of the halostad was accompanied by a corresponding shallowing of the Atlantic water layer traced by the 0 °C isotherm. From the end of June to mid-September, the 0 °C isotherm shallowed from 145–150 to 125–130 m (Figure 7b), and the isohaline 34.5 was correspondingly uplifted by ~20 m (Figure 7c).

During the transition period, the CDOM concentration was significantly lowered through the entire water column (Figure 7d). Through the halostad and underlying halocline, CDOM was reduced from ~105–107 to 95–100 ppb and from 105 to 85–90 ppb, respectively. The CDOM reduction in the sub-ice water layer was similar to the halocline. In the Atlantic Water layer, CDOM was lowered from ~80–85 to 70–75 ppb.

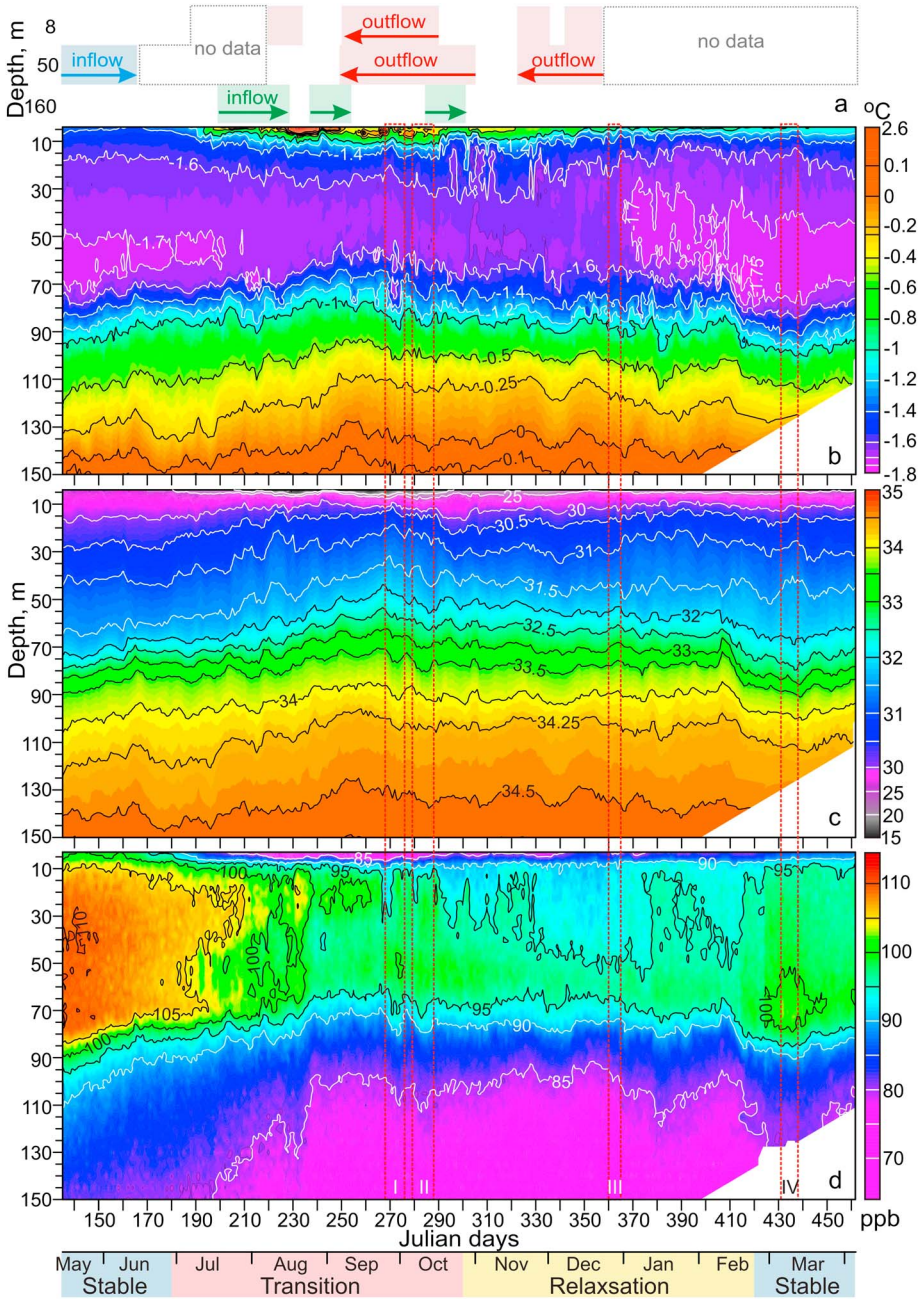

Figure 7. (a) Schematic depictions show the on-shelf inflow (blue and green shading and arrows) and outflow (pink shading and red arrows) events based on ADCP data for (top) 8, (middle) 50, and (bottom) 160 m depth. (b) Temperature (°C), (c) salinity, and (d) Colored Dissolved Organic Matter fluorescence (ex/em 370/460 nm, ppb) from the Ice Tethered Profiler deployed over the southeastern Wandel Sea shelf from 15 May 2015 to 6 April 2016. Red-dashed rectangular indicates storm events associated with southerly and southwesterly winds over the Wandel Sea continental slope with their reference numbers from I to IV at the bottom. Color shading at the bottom highlights different periods of conductivity-temperature-depth and Colored Dissolved Organic Matter variability.

Synoptic variability at the ~8- to 10-day time scale drove the most significant disturbances of the CTD and CDOM profiles during two separate events I and II that were identified at the end of the transition period from velocity data (red-dashed rectangular in Figure 7). Both events show similar CTD and CDOM structure: saltier, cooler, and less CDOM water at the upper part of the halostad from the beginning of the events followed by fresher, cooler, and high CDOM water at the lower part of the halostad. We also note that for the halostad, the mooring time series for the transition period is consistent with the modifications observed

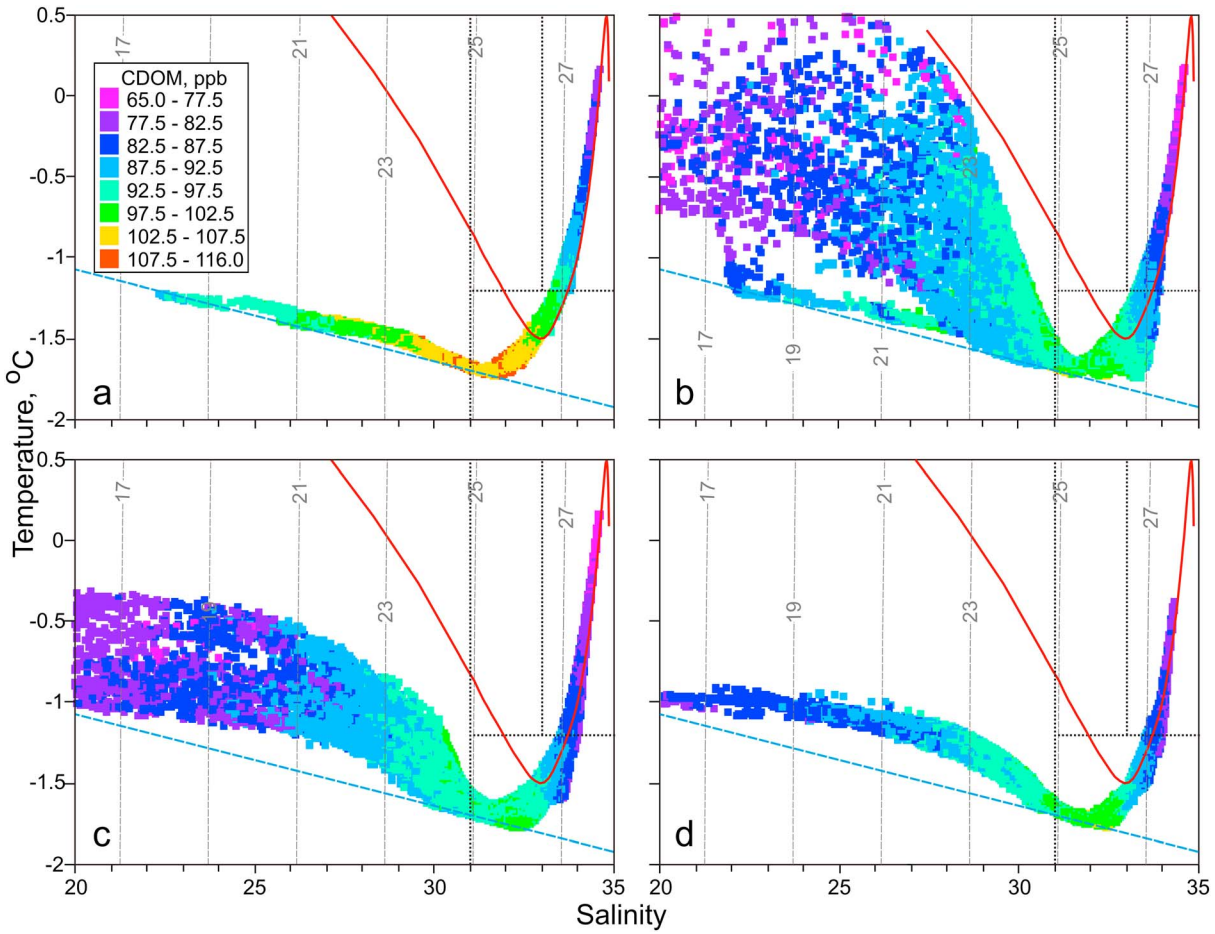

Figure 8. In situ *TS* scatterplots of the temperature, salinity, and Colored Dissolved Organic Matter time series from the mooring during (a) stable, (b) transitional, (c) relaxation, and (d) stable periods. Colored Dissolved Organic Matter fluorescence (ppb) is shown in color. The gray dashed lines are potential isopycnals in kilogram per cubic meter. The dashed blue line is surface freezing temperature. Black-dotted lines indicate the bounds defining the different water masses in the western Beaufort Sea following von Appen and Pickart (2012): The 33 line separates the Pacific ($31 < S < 33$) from the Atlantic ($S > 33$) water, and the −1 °C line separates the Pacific summer and winter water. Red line shows in situ mean *TS* diagram for the cross-slope eastern Beaufort Sea section adopted from Dmitrenko et al. (2016).

between the CTD profiles from April–May to the end of August (Figures 5a–5e). Both the CTD and ITP data show salinification throughout the entire halostad layer, while a freshening tendency from winter to summer can be expected due to snow, ice, and glacier melt as observed for the sub-ice water layer where salinity decreased from >25 in May–June to 17–20 in August–October (Figures 7b and 7c).

The relaxation period is characterized by a gradual return to the initial CTD conditions of May–June 2015 (Figures 7b and 7c) after termination of the Atlantic water on-shelf flow at the end of October 2015 (Figures 6c and 7a). The under-ice water layer cools down to approximately −1 °C at salinity ~25. The lower boundary of the halostad and the halocline water layer were deepened to about the same depth as May–June 2015. This tendency is obvious since JD370 when the low part of the halostad at 70 m depth started to cool down to −1.75 °C and freshened by ~1. At this time, CDOM showed a gradual reduction through the upper halostad, and only the low halostad maintained the CDOM values typical for the end of the transition period.

The stable period from February to April 2016 was characterized by higher salinity (~0.5) and lower CDOM (~7 ppb) compared to what was observed in May–June 2015. For example, during the first 10 days of March 2016 at 60 m depth, the lower part of the halocline was saltier by ~0.4, but almost at the same temperature (approximately −1.7 °C) as in May 2015. This result is consistent with CTD profiles taken along the glacier trough in April 2016. Overall, from May 2015 to April 2016 the halostad became saltier while CDOM declined. This suggests a relationship between salinity and CDOM through the halostad depth range.

The TS scatterplots of the temperature, salinity, and CDOM time series from the ITP shows the seasonal evolution of the CDOM maxima in the *TS* space (Figure 8). From the stable to transitional period, the CDOM maxima became saltier (by ~1) and denser (by ~0.5 kg/m^3)—Figures 8a and 8b. During the relaxation period, a gradual return to the initial thermohaline conditions of the CDOM maxima is observed (Figures 8c and 8d), but the CDOM values are reduced by ~10 ppb (Figures 7 and 8).

Overall, the results derived from the ITP data for depths exceeding 15 m are consistent with a seasonal cycle observed through the halostad, halocline, and underlying Atlantic water layer over the southeastern Wandel Sea shelf. From May to October, the lower boundary of the halostad is shallower, and the halostad is warmer, saltier, and has a lower CDOM concentration. We refer to this pattern as the halostad summer mode. We also recorded that the halostad was consistent with the summer mode in April–May 2015 over the western flank of the glacier trough. During summer, the Atlantic water layer is elevated, warmer, and saltier. In contrast, from January to May, the low boundary of the halostad is deepened, and the halostad is cooler, fresher, and the CDOM is enriched. We refer to this modification as the halostad winter mode. The winter mode of the halostad was observed in both April–May 2015 and April 2016 over the glacier trough at a distance from the tidewater glacier terminus. During winter, the Atlantic water layer is deeper, cooler, and less saline. In general, the summer mode is associated with on-shelf inflow of the Atlantic water and outflow of the overlaying halostad water. In contrast, the winter mode is related to the on-shelf inflow of the halostad water.

4. Discussion

4.1. Assessment of the Seasonal Cycle Based on Areal Data and Mooring Observations

We suggest that the seasonality in water column properties in the southeast Wandel Sea below the under-ice meltwater layer is generated by the onshore lateral displacement of the coastal branch of the PW outflow from the Arctic Ocean to the western Fram Strait driven by the annual cycle in wind forcing observed over the Wandel Sea continental slope. Seasonality of the solar radiation has little influence on the intermediate water layer, which is isolated year-round from the surface by the subsurface halocline with exceptionally strong salinity (density) stratification (Bendtsen et al., 2017; Dmitrenko et al., 2017; Kirillov et al., 2018). Further indication of its isolation from the surface water is that during summer the water layer below 15 m depth exhibits salinification, while freshening is expected due to snow, sea-ice, and glacier melt. This is most likely due to advection of the seasonal signal from upstream with the Pacific-derived Arctic water flow along the Greenland coast.

Following Dmitrenko et al. (2017), we attribute the Wandel Sea halostad layer to the Pacific-derived Arctic water. For 2008–2009 over the upstream Lincoln Sea area (Figure 1), de Steur et al. (2013) reported on PW at 32.5–33.5 salinity as cold as −1.65 °C. In the Canada Basin, the Upper Halocline Water with temperatures down to −1.5 °C at salinities of ~32–33, originating from the Chukchi Sea shelf (Timmermans et al., 2017), is likely comprised by the Pacific winter water. Over the western (Alaskan) Beaufort Sea, water with the salinity $31 < S < 33$ is generally assigned to PW (von Appen & Pickart, 2012). This definition is also applicable for the eastern (Canadian) Beaufort Sea (Dmitrenko et al., 2017). The haline properties of the Wandel Sea halostad are generally in line with these definitions (Figure 8). They are also consistent with ~32.2 salinity of the Pacific-derived Arctic water in Fram Strait reported by Jones et al. (2003). However, the salinity of the Wandel Sea upper halostad (~20–25 m depth) of ~30 is too low to be assigned to PW. Moreover, the temperature of the Wandel Sea lower halostad (~60–70 m depth) of −1.75 °C is too low to be assigned to the Pacific Winter water. Thus, PW has been modified en route through the Arctic Ocean to northwest Fram Strait. The low-salinity shelf water from the Siberian shelves modifies PW either across the Chukchi Sea or crossing over the Lomonosov Ridge into the Makarov Basin and eventually entering the Canada Basin (Morison et al., 2012). The lower halostad temperature close to the freezing implies that PW has been recently ventilated from the surface during winter en route to the Wandel Sea. This also confirms the remote origin of the halostad. The southeastern Wandel Sea shelf is landfast ice covered and stratified all year round preventing ventilation of the water column locally (Bendtsen et al., 2017; Dmitrenko et al., 2017).

The Pacific origin of the Wandel Sea halostad is also confirmed by the elevated values of the CDOM fluorescence (Figure 7c). CDOM in the Arctic originates predominantly from terrigenous organic matter primarily attributed to the Eurasian and American continental runoff water (Amon et al., 2003; Stedmon et al., 2011)

as well as to interactions with sediments on the Arctic shelves (Guéguen et al., 2007; Stedmon et al., 2011). The CDOM fluorescence maxima in the halostad is consistent with results from the Canada Basin where this maximum is attributed to the PW of winter origin (Guéguen et al., 2007) and the continental river runoff water (e.g., Granskog et al., 2012). For the downstream NEW area, Amon et al. (2003) reported the two intermediate maxima of the CDOM fluorescence: through the shelf halostad layer and continental slope at salinities of ~32.0–32.5 and ~33.0–33.5, respectively, and temperature of approximately −1.7 °C (see also Falck, 2001). This could be a differentiation between the PW CDOM and CDOM from the Siberian Rivers. The NEW shelf maximum resembles the TS characteristics of the CDOM maximum in the Wandel Sea (Figure 8).

The CDOM over the Wandel Sea shelf shows the seasonal patterns consistent with those for temperature and salinity (Figures 7 and 8). During summer, the reduced CDOM maximum is associated with saltier (by ~1), denser (by ~0.5 kg/m^3), and shallower water layer (Figures 7, 8b, and 8c). In context of the results by Amon et al. (2003), we speculate that the winter CDOM maxima in the lower halostad (Figures 8a and 8d) is likely from the PW passage over the Chukchi Sea shelf rather than the Siberian river runoff passage with Transpolar Drift.

What causes the seasonal-like behavior of the Pacific-derived halostad? PW in the Arctic Ocean clearly shows seasonality. There are strong seasonal variations in the thermohaline signal upstream in the Bering Strait where PW inflows to the Arctic Ocean (Woodgate et al., 2005, 2012). Over the Chukchi and western Beaufort seas, PW shows summer and winter mode based on its formation. The summer PW with temperatures above −1.2 °C and salinities between 31 and 32 (Steele et al., 2004) is usually composed of the Chukchi Summer Water (Woodgate et al., 2005) and the Alaskan Coastal Water (Pickart et al., 2005). Below the summer PW is a layer of winter PW that can be as cold as −1.45 °C and forms during winter sea-ice formation within the Bering and Chukchi shelves (Jones & Anderson, 1986; Pickart et al., 2005; Weingartner et al., 1998). The advection of the Pacific winter water is also tied to seasonality of the Bering Strait inflow to the Arctic Ocean (Shroyer & Pickart, 2018). Overall, it should come as no surprise that a seasonal signal in the PW properties can maintain its identity downstream over the Canada Basin and Canadian Beaufort Sea. For example, the seasonal signal in the Arctic Ocean AW boundary current at depths exceeding 180–200 m maintains its identity along the Nansen Basin Siberian margin ~2,500 km downstream from the source area in eastern Fram Strait (Dmitrenko et al., 2009; Lique & Steele, 2012). For the Canada Basin using a year-long CTD record (2009–2010) from a drifting ITP, Timmermans et al. (2017) reported on the seasonal cycle through the halocline layer, which is consistent with that recorded by our mooring in the Wandel Sea. However, the cold halocline in the Canada Basin with temperatures of −1.5 °C to −1.75 °C was found deeper (110–230 m depth) compared to the Wandel Sea. The PW seasonal modulation can be expressed as alternation between summer and winter PW that is, in general, consistent with alternation between summer and winter modes of the Wandel Sea halostad. It is possible, however, that the observed seasonal changes over the southeast Wandel Sea shelf are instead governed by a wind-driven seasonal shift of the PW boundary current relative to the shelfbreak, as was described for the AW boundary current along the Siberian continental slope by Dmitrenko et al. (2006).

For duration of field operations at Station Nord in 2015–2016, the time series of the 24-hr mean wind were generated using the NCEP data set (Figures 9a and 9b). Zonal and meridional 10-m wind data were derived for the Wandel Sea continental slope ~35 km from the mooring (Figures 2a, 4a, 9c, and 9d). In general, the landfast ice cover eliminates the surface wind stress. However, for the landfast ice-covered areas over the Greenland coast in ~20–50 km to the landfast ice edge, the wind-forced circulation can be induced by upwelling and downwelling developed at the vicinity of the landfast ice edge (Dmitrenko et al., 2015; Kirillov et al., 2017).

It seems that the on-shelf inflow of the halostad water is controlled by the downwelling-favorable northerly winds. The storm event driven by northerly winds up to 15 m/s occurred in the third 10-day period of April 2015 (JD112–114, Figures 9a and 9b). The short-term mooring deployed at the front of tidewater glacier terminus recorded the on-shelf inflow through the water layer down to ~50 m depth and outflow in the layer beneath, which is consistent with downwelling (Kirillov et al., 2017). Before 30 May 2015 (JD150), the ADCP velocity data from 50 m depth (Figure 6b) show relatively weak on-shelf inflow with a mean velocity of 2.2 cm/s. In contrast, during the following 6 days the onshore transport increased more than twice up to

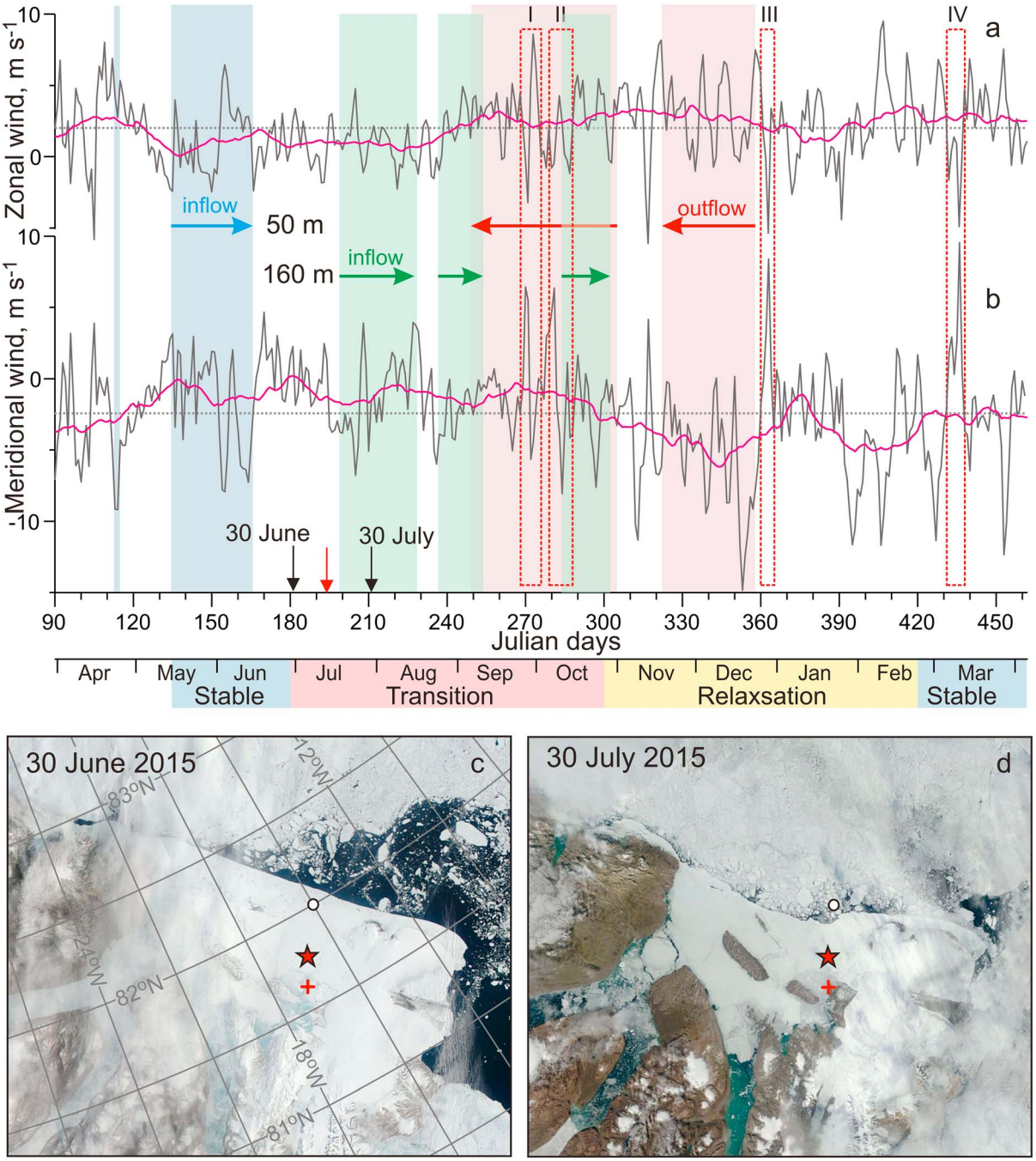

Figure 9. Time series of the National Centers for Environmental Prediction-derived 24-hr mean 10-m (a) zonal and (b) meridional wind (m/s) over the Wandel Sea continental slope at 82°N, 15°W (position depicted by white circles in c–d) from April 2015 to April 2016. Purple line shows the 30-day running mean. Blue and green shading and arrows highlight the on-shelf inflow at 50 and 160 m depth, respectively. Pink shading and red arrows highlight shelf outflow at 50 m depth. Red-dashed rectangular indicates storm events associated with southerly and southwesterly winds over the Wandel Sea continental slope with their reference numbers at the top. Color shading at the bottom highlights different periods of conductivity-temperature-depth and Colored Dissolved Organic Matter variability as of Figure 7. Red arrow at the bottom identifies the day when the landfast ice was collapsed over the Wandel Sea continental slope. The MODIS/TERRA satellite images show the evolution of the landfast ice from (c) 30 June to (d) 30 July 2015. Red circle and cross depict mooring and SN, respectively.

5.2 cm/s. This enhancement is clearly attributed to the northerly wind events during JD151–156 (Figure 9b). Note, however, that since May 2015 the mean atmospheric forcing changed to the upwelling-favorable southerly winds dominated to the mid-October 2015 (Figure 9b).

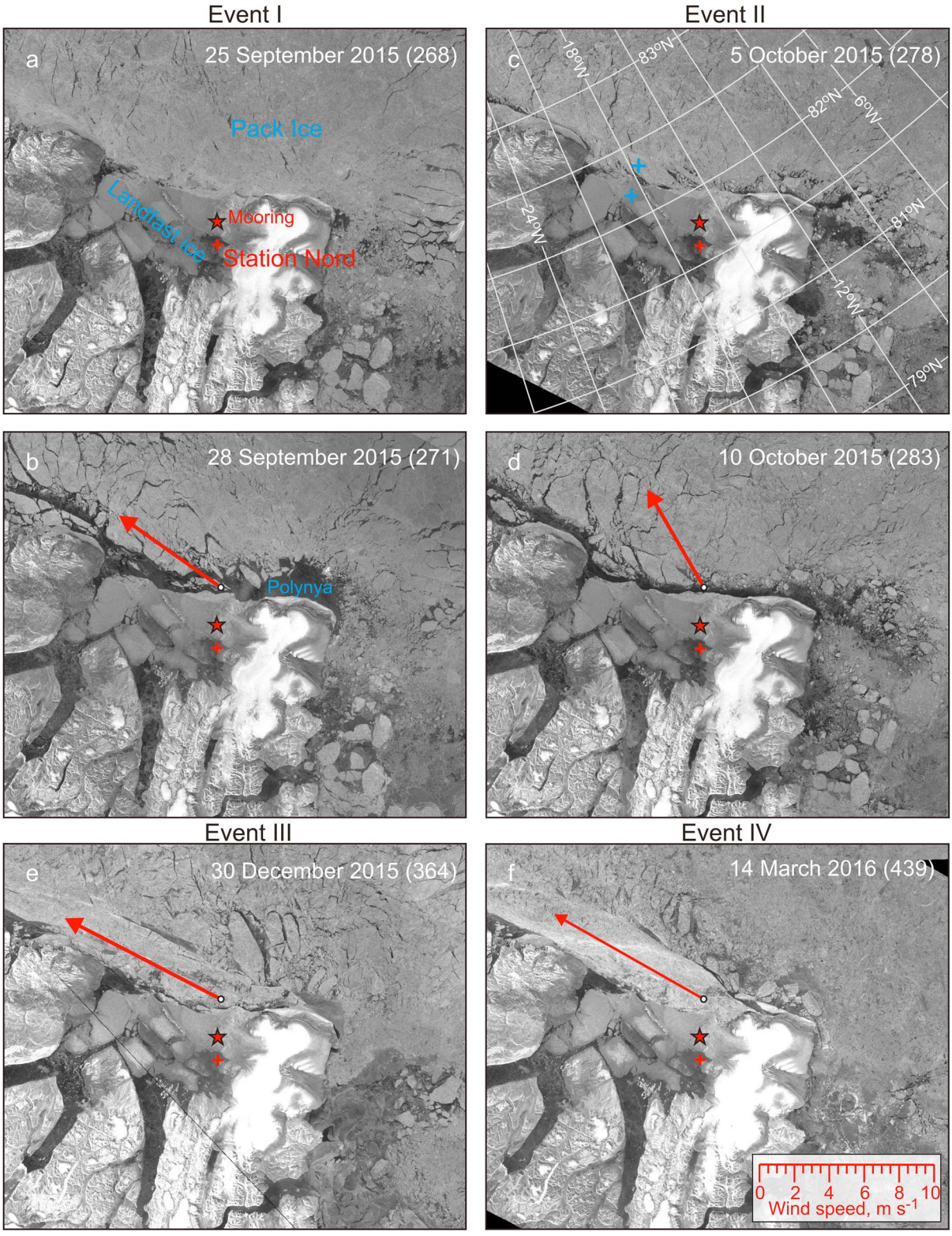

Figure 10. The Sentinel-1 C-band SAR images taken over the Wandel Sea and Northeast Water Polynya at the beginning of storm events # (a) I and (c) II and 24-hr following the meridional wind maxima over the Wandel Sea continental slope for storm events # (b) I, (d) II, (e) III, and (f) IV. Red arrows indicate the 24-hr mean direction and velocity of maximal wind according to scale shown in (f). Red star and cross depict mooring and SN, respectively. (c) Blue crosses indicate positions over the Wandel Sea outer shelf and continental slope where the time series of the Pacific Water tracers shown in Figures 12c and 12d, respectively, were taken.

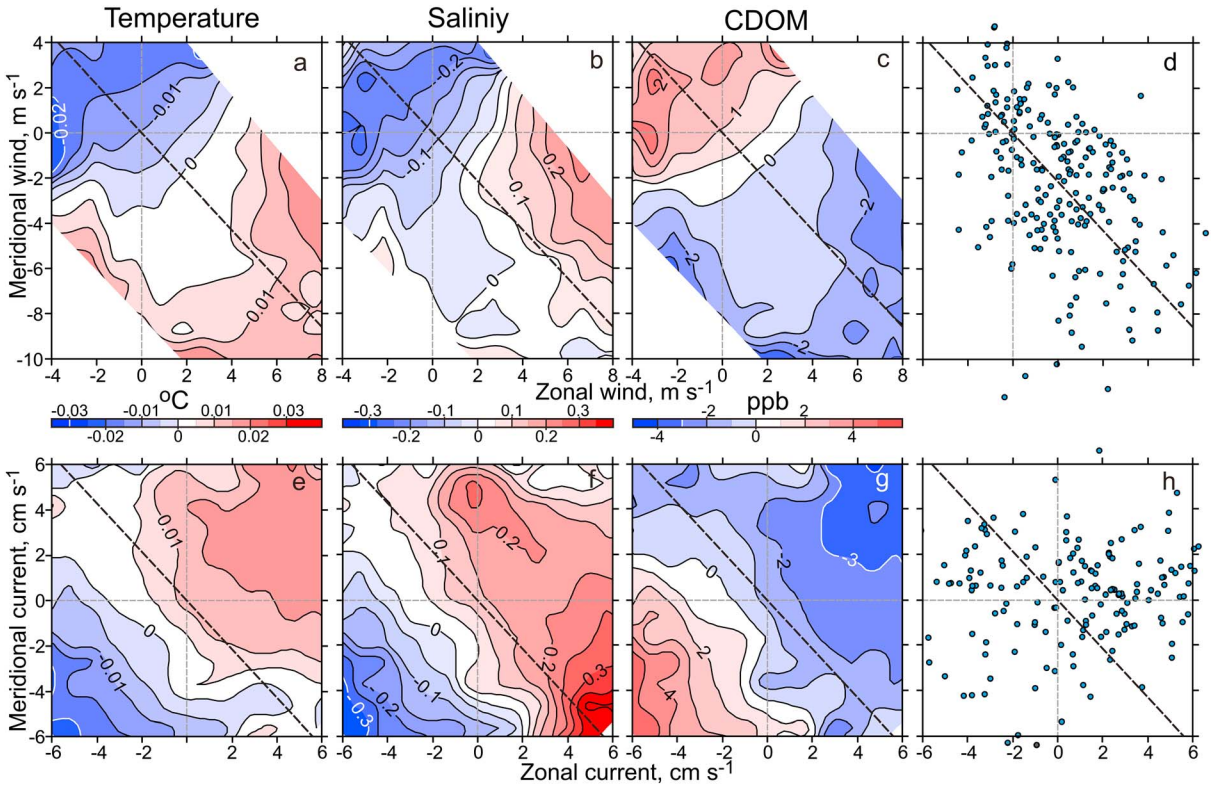

Figure 11. Color shading shows daily mean (a, e) temperature (°C), (b, f) salinity, and (c, g) CDOM (ppb) anomalies at 50 m depth from the moored Ice Tethered Profiler versus National Centers for Environmental Prediction daily mean 10-m wind over the Wandel Sea continental slope (top) and daily mean currents at 50 m depth (bottom) from 15 May to 26 December 2015. Scatter plots show daily mean (d) winds and (h) currents used for computing (a)–(c) and (e)–(g), respectively. Black dashed line depicts the along-slope direction derived from the International Bathymetric Chart of the Arctic Ocean. CDOM = Colored Dissolved Organic Matter.

For the upwelling-favorable wind forcing, the AW on-shelf inflow is expected along with outflow through the overlaying halostad and under-ice water layers. In fact, the on-shelf AW flow along the glacier trough was observed following the upwelling-favorable storms in JD170–190 by about 1 month (Figure 9b). We speculate that this delay is attributed to the landfast ice extending eastward beyond the shelfbreak suggesting that upwellings are sensitive to the sea-ice conditions over the continental slope. The Wandel Sea is the only place in the high Arctic where the landfast ice can extend over the shelfbreak and upper continental slope. The satellite imagery shows that since mid-December 2014 the landfast ice edge, controlled by northerly winds through a surface Ekman onshore transport, was gradually extending eastward (not shown) and in mid-March 2015 it was finally stabilized over the Wandel Sea upper continental slope (e.g., Figure 9c). On 13 July 2015 (JD194) the outer part of the landfast ice area collapsed, and the landfast ice edge resided onshore by ~17 km beyond the shelf break (Figure 9). Five days later starting 17 July (JD198), the AW on-shelf flow was established in response to the upwelling-favorable southerly wind forcing. This result suggests that there is no an Ekman response to wind forcing when the landfast ice extends over the shelf break. This is consistent with results by Carmack and Chapman (2003). Based on numerical simulations of shelf-basin exchange, they reported on abrupt onset of the shelfbreak upwelling when the ice edge retreats beyond the shelfbreak.

From the end of October 2015 to the end of the mooring record in April 2016, the atmospheric forcing was again dominated by the downwelling-favorable northerly winds (Figure 9b). For the downwelling-favorable storms in November 2015 (JD311–322), the outflow at 50 m depth was reversed to westward direction, which is more consistent with on-shelf inflow driven by downwelling. However, later on the northeast flow was retained, while northwestward flow is expected to continue as far as the downwelling-favorable wind forcing is imposed, that is, until the end of February 2016 (Figure 9b). We are unable to evaluate the halostad water dynamics after 26 December 2015 when the ice-tethered ADCP stopped working. However, we note that as soon as southerly winds over the Wandel Sea continental slope were reversed on ~JD300, the AW inflow along the glacier through was terminated.

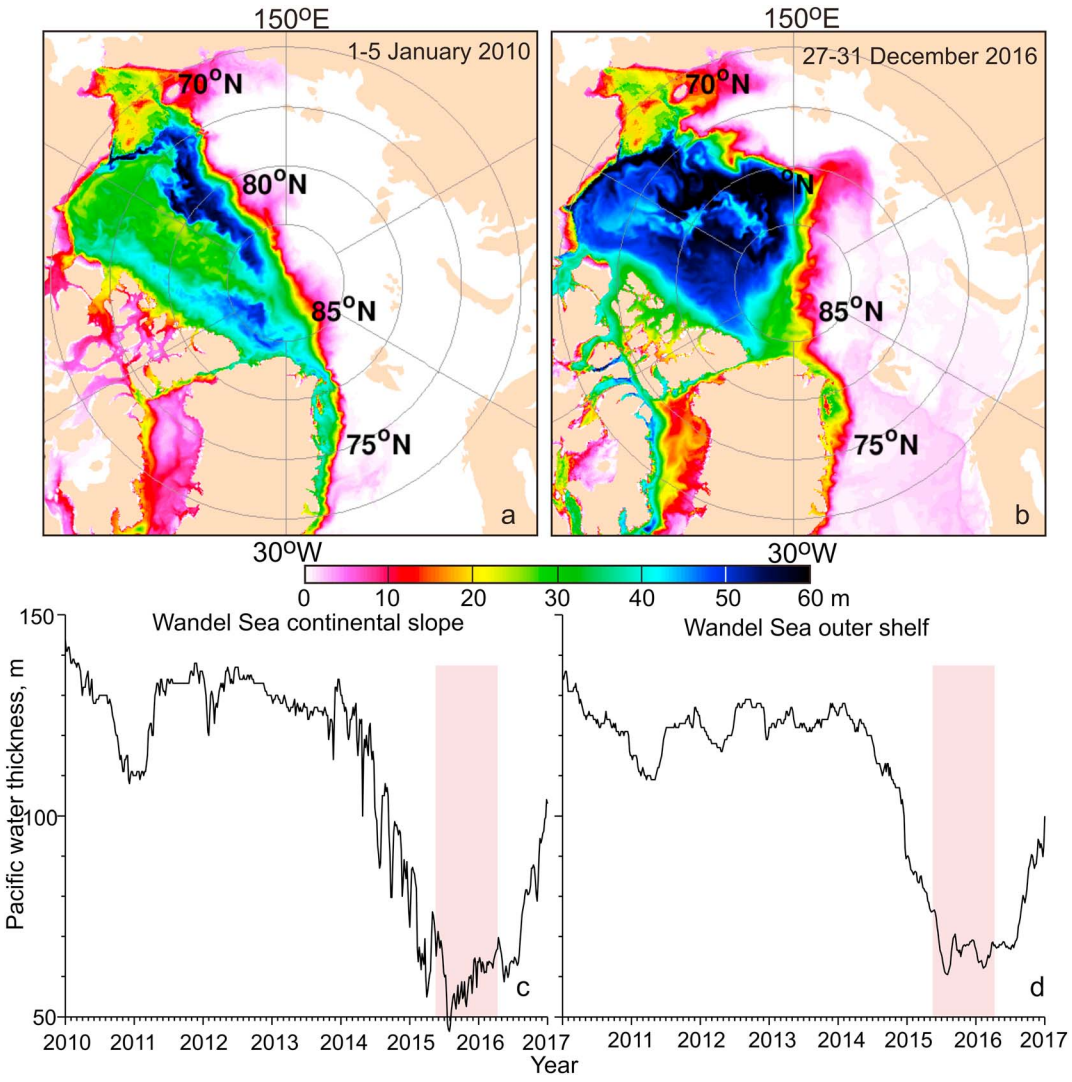

Figure 12. Simulated Pacific Water tracers concentration (m) for (a) 1–5 January 2010 and (b) 27–31 December 2016 and time series of the Pacific Water tracers integrated through the 20–85 m depth layer over the Wandel Sea (c) continental slope at 82°20′N, 17°40′W and (d) outer shelf at 82°10′N, 18°40′W (positions are depicted in Figure 10c). (c, d) Pink shading highlights period of mooring record.

To evaluate in more details the response of the water column to wind forcing, we specifically focused on four upwelling-favorable storms in September–October 2015 (#I and II), and during the end of December 2015 (#3) and mid-March 2016 (#4). Among these four storms, #III and IV were the strongest, with maximal southerly winds up to 10.0 (29 December 2015, JD363) and 11.2 m/s (11 March 2016, JD436), respectively —Figures 9b and 10b–10f. For storms in September–October 2015, the upwelling-favorable southerly wind forced the pack ice off the landfast ice edge, and a polynya was developed over the upper continental slope (Figures 10a–10d). This wind, however, was reversed, lagging southerly wind maximums by 2–4 days (Figure 9b). For storm events in December 2015 and March 2016, the landfast ice was recorded extending over the Wandel Sea continental slope, and the ice edge was not extensively modified during these storms (Figures 10e and 10f).

Events III and IV show no significant CTD and CDOM variability that can be attributed to wind forcing (Figure 7). As of our preceding discussion on the delay of upwelling onset in response to summer upwelling-favorable wind forcing, we attribute this to the landfast ice extension over the upper continental slope (Figures 10e and 10f). In contrast, events I and II show significant modifications in response to wind forcing in a similar way for both events. From the beginning, through the upper halostad layer (~15–45 m depth) the CDOM was lowered by ~8–10, and salinity increased by ~0.2. This is consistent with east-

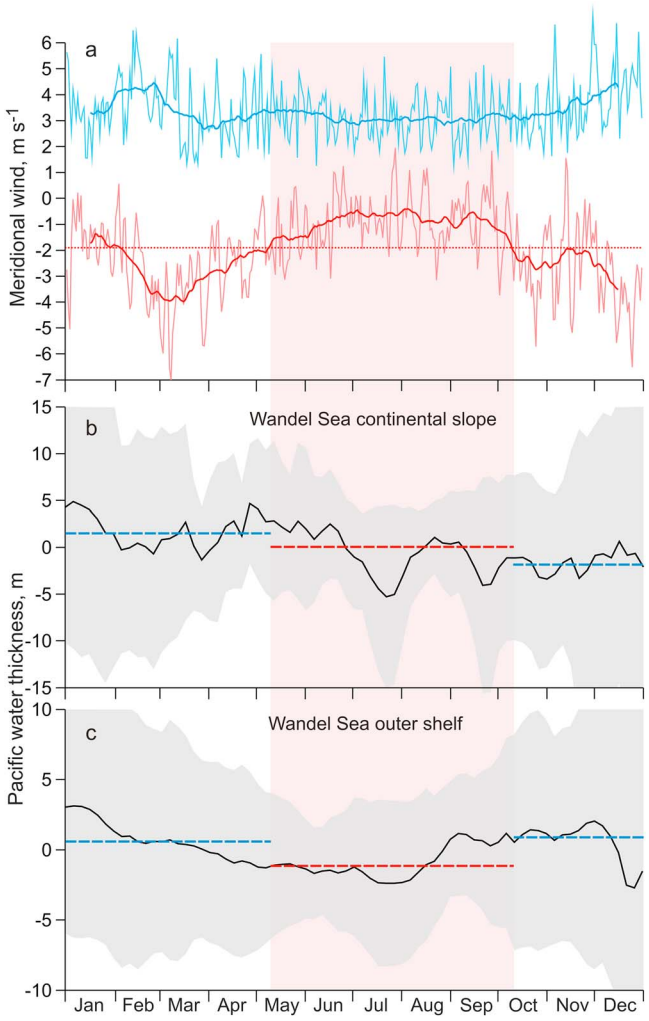

Figure 13. (a) National Centers for Environmental Prediction-derived 7-year mean (2010–2016) 10-m meridional wind (pink, m/s) over the Wandel Sea continental slope with its standard deviation on the top (blue). Blue and red thick lines show the 30-day running mean. The 7-year mean (2010–2016) anomalies of the simulated Pacific Water tracers concentration anomalies (m) integrated through the 20–85 m depth layer over the Wandel Sea (b) continental slope and (c) outer shelf. Gray shading highlights ±1 standard deviation. Pink shading highlights period dominated by southerly winds. Red and blue dashed lines show mean for periods dominated by southerly and northerly winds, respectively.

southeastward transport (Figures 6a and 6b) of the midshelf water less affected by the Pacific-derived Arctic water. In ~4–5 days following this modification, at the lower depths (70–90 m) water became fresher (by ~0.3), cooler (by 0.2–0.4 °C), and higher in CDOM (by ~5)—Figure 7. This is consistent with deepening of the halostad in response to the downwelling-favorable northerly winds lagging behind the upwelling-favorable wind forcing by ~2–4 days.

Following Dmitrenko et al. (2017), we assume that the source of the halostad water is located over the Wandel Sea shelfbreak and upper continental slope, that is, the area of the coastal branch of the Pacific-derived Arctic water flowing along the northeast Greenland coast. To confirm the source of the halostad water we use the 3-D CTD/CDOM-winds and CTD/CDOM-currents scatter analysis carried out using mooring-derived ITP and ADCP data at 50 m depth and NCEP-derived 10-m wind over the Wandel Sea continental slope—Figure 11. The scatter plots for wind (Figure 11d) and current (Figure 11h) illustrate confidence of the scatter analysis in Figures 11a–11c and 11e–11g for variety of winds and currents. Scatter analysis of temperature, salinity, CDOM records, and wind shows that southeasterly along-slope winds are generally associated with lower temperatures, lower salinity, and higher CDOM at the mooring location. This is consistent with on-shelf Ekman transport of these anomalies from the continental slope. In contrast, the northwesterly winds are attributed to warmer, saltier, and less CDOM-rich water assuming the off-shelf Ekman transport originated from the Wandel Sea midshelf (Figures 11a–11c). The average rate of temperature, salinity, and CDOM anomalies related to change in wind patterns is estimated at ±0.15 °C, ±0.2, and ± 2 ppb, respectively. Scatter analysis of temperature, salinity, and CDOM records versus currents clearly indicate the source of anomalies recorded by mooring (Figures 11e–11g). The northeastward flow caries warmer, saltier, and less CDOM water from the midshelf. The southeastward flow transports cooler, fresher, and CDOM-enriched water from the shelfbreak. The associated mean anomalies of temperature, salinity, and CDOM are similar to those driven by wind (Figures 11e–11g).

The general assessment of wind forcing, water dynamics, CTD areal survey data, and CTD and CDOM mooring data explains the spatial and temporal variability of the halostad water layer over the southeast Wandel Sea shelf. During winter, the northerly downwelling-favorable winds force the halostad water to flow on-shelf, comprising the winter mode of the Pacific-derived halostad over the Wandel Sea outer shelf (Figures 6b, 7, and 9b). The southerly upwelling-favorable winds in July–October induce shelf outflow through the halostad water layers (Figures 6a, 6b, and 9b). For the subsurface layer, the northeast flow in August–October favors transport of a relatively warm melt water from the ice-free area to the outer shelf covered by multiyear landfast ice (Kirillov et al., 2017). It is confirmed by mooring CTD and velocity data (Figures 6a and 7). During this time the halostad winter mode was subsidized with summer mode recorded in April–May 2015 to the southeast of our mooring (Figures 5a–5e) suggesting lateral offshore displacement of the winter halostad in response to upwelling. The upwelling of modified AW along the glacier trough caused the inflow of warmer and saltier water, and the entire thermohaline structure of water below the subsurface halocline has been uplifted (Figures 6c and 7). The salinification also observed over the western flank of the glacier trough seems to be attributed to both elevating of isohalines caused by upwelling and the offshore residing of winter halostad. The landfast ice extending during winter over the Wandel Sea shelfbreak and upper continental slope damps upwelling, which starts to develop as soon as the outer portion of the landfast ice is collapsed.

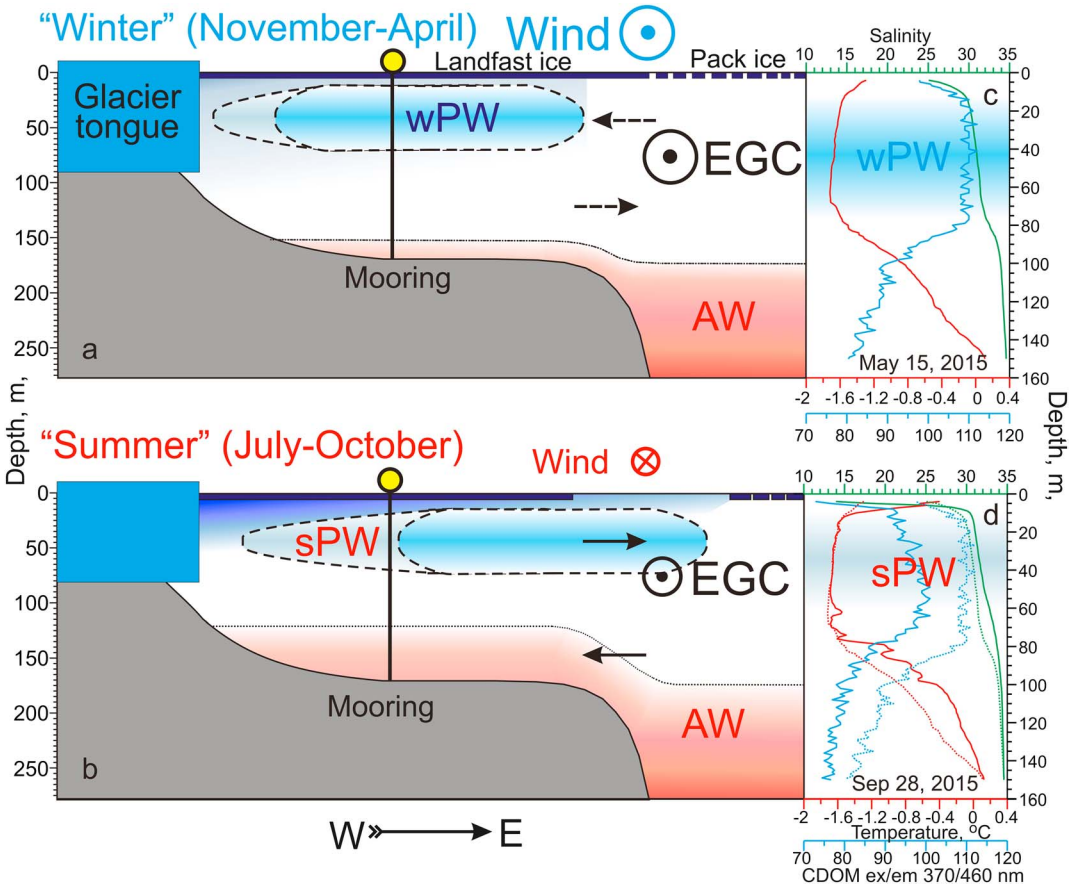

Figure 14. Schematic depictions suggest lateral displacement of the Pacific-derived halostad in response to (a) "winter" (November–April) northerly and (b) "summer" (May–October) southerly wind forcing over the Wandel Sea continental slope with corresponding Ice Tethered Profiler conductivity-temperature-depth and CDOM vertical profiles shown in (c) and (d), respectively. (d) Dotted lines show summer profiles for comparison. Winter (cooler, fresher, and CDOM-enriched) and summer (warmer, saltier, and less CDOM) modes of Pacific-derived halostad are identified as (a, c) wPW and (b, d) sPW, respectively. CDOM = Colored Dissolved Organic Matter.

4.2. Assessment of the Seasonal Cycle Based on Numerical Simulations

The preceding analysis motivated us to use an experiment of a high-resolution numerical model to assess the PW flow along the Wandel Sea upper continental slope and its seasonal variability. A passive tracer was introduced into the model at Bering Strait from the beginning of the experiment on 1 January 2002. A snapshot of the passive tracer fields in January 2010 shows that the model reproduces two pathways of the PW flow (i) following the Beaufort Sea continental slope and (ii) crossing the Arctic Ocean to Fram Strait (Figure 12a) in agreement with a schematic circulation of PW in Figure 1. In the western Fram Strait and Greenland Sea, the PW tracers are distributed southward along the Greenland shelf and continental slope with concentration of PW up to 45 m over the Wandel Sea shelfbreak. This tracer distribution is consistent with previous modeling by Hu and Myers (2013) and Aksenov et al. (2016). Further integration to December 2016 revealed accumulation of PW in the Canada Basin and corresponding decrease of the PW outflow through western Fram Strait (Figure 11b). This corroborates results by Brugler et al. (2014) showing that in recent years a significant portion of PW has been advected into the interior Canada Basin. Zhong et al. (2018) suggested that the changing pathways of PW are related to the changing position of the Beaufort Gyre and the intensification of geostrophic currents in the southwestern Canada Basin. Recently, Dmitrenko et al. (2018) highlighted the role of the wind-forced upwellings and downwellings over the Beaufort Sea continental slope to explain the alternating pathways of PW in the Arctic Ocean. The PW accumulation in the Canada Basin from 2010 to 2016 results in a decrease of the PW tracers over the Wandel Sea upper continental slope down to ~20 m (Figure 12b). By July 2015 over the Wandel Sea outer shelf and upper

continental slope, the PW tracers integrated through the 20–85 m depth were reduced to 61 and 47 m, respectively (Figures 12c and 12d).

The simulated seasonal cycle over the Wandel Sea outer shelf and upper continental slope was explored using the 7-year mean seasonal anomalies generated for the two positions depicted in Figure 10c. The seasonal anomalies were obtained by computing a representative year. For each year, the mean was estimated, and then the anomalies for a given date were derived along with standard deviations. Finally, they were averaged from 2010 to 2016 for the Wandel Sea continental slope (Figure 13b) and outer shelf (Figure 13c). For both the outer shelf and continental slope the PW variability is higher during winter and lower during summer. It is likely due to a more persistent summer atmospheric forcing dominated by sustainable southerly winds (Figure 13a). Over the upper continental slope the seasonality of the PW tracer's anomalies is very limited (Figure 13b). In contrast, over the outer shelf the seasonal cycle is traceable, but not statistically confident, partly due to significant variability of the PW anomalies during winter. Note that the model does not take into account the landfast ice extension over the upper continental slope during late winter, as we discuss below. The shelf-to-slope difference in seasonal cycling suggests that the seasonal signal is generated locally rather than advected from the Canada Basin. Overall, the numerical simulations reveal that (i) PW occupies the Wandel Sea outer shelf as also evident from our mooring observations and (ii) the PW seasonal cycle is generated locally due to the seasonality of wind over the Wandel Sea continental slope (Figure 13a) and associated Ekman transport of PW. While the results of model simulations are not capable of fully reproducing the PW seasonal cycle over the outer shelf, they are entirely consistent with conclusions obtained using observational data on CTD, CDOM, and currents.

5. Summary and Conclusions

Over the Canada Basin, PW impacts the halocline structure, producing a double halocline with a cold Halostad formed by the volumetric injection of Pacific winter water. The ITP data from the Wandel Sea shelf revealed that the subsurface (~15–85 m depth) low stratified cold halostad with salinities of 30–31.5, temperatures down to −1.7 °C, and high CDOM values resembles the cold Halostad in the Canada Basin. Our results suggest that the Wandel Sea halostad is maintained by the on-shelf inflow of PW modified en route to Fram Strait and advected along the Wandel Sea shelfbreak and upper continental slope by the PW outflow from the Arctic Ocean.

Wind forcing over northeastern Greenland shows a northerly component during winter that favors Ekman transport of the Pacific-derived Arctic water to the Wandel Sea outer shelf (Figure 14a). As a result, a higher fraction of the Pacific-derived water significantly modifies the outer shelf water column; the halostad is cooled, freshened, and CDOM-enriched, and its lower boundary is deepened (Figures 14a and 14c). The northerly winds also favors the sea-ice Ekman transport conditioning the landfast ice extension over the Wandel Sea shelfbreak and upper continental slope (Figure 14a).

The prevailing southerly summer winds favor upwelling that results in retreat of the Pacific-derived water off the shelf, but also forces the on-shelf inflow of Atlantic water (Figure 14b). The halostad lower boundary is shallowed, and halostad becomes saltier, warmer, and CDOM is reduced, indicating the lower fraction of the Pacific-derived water on the shelf (Figures 14b and 14d). During winter the landfast ice extends over the upper continental slope and disrupts the wind-driven seasonal patterns. The position of the landfast ice edge relative to the shelf slope break illustrates the important role which landfast ice can play in coastal upwelling, consistent with modeling of Carmack and Chapman (2003), and observations at other landfast ice edge locations (e.g., Tremblay et al., 2011). Once the landfast ice has collapsed, the upwelling favors the Atlantic water on-shelf inflow accompanied by the PW outflow as indicated in Figure 14b.

The seasonal patterns of the Pacific-derived water over the Wandel Sea shelf are in agreement with results of the CTD survey and numerical simulations. Simulations of the PW tracers suggest a role of the local wind forcing for the PW on-shelf inflow during winter, but the results on simulated seasonality are not statistically significant. It seems that the deficiencies of the model simulations are conditioned by an incomplete definition of the landfast ice pointing out a necessity for more realistic sea-ice parametrization and higher spatial resolution over the Wandel Sea continental slope area. Seasonality of the wind is the hypothesized cause of the halostad variability, but probably does not provide a complete explanation. Several other mechanisms, including dynamical instabilities and seasonal features of the east Greenland current (e.g., Bacon et al.,

2002), may contribute to the lateral displacement of the PW flow relative to the Wandel Sea shelfbreak and upper continental slope. Future research in this hard to access region will help clarify our findings.

Acknowledgments
This study was funded by the Canada Excellence Research Chair program (SR), the Canada Research Chair program (DB), the Canada Foundation of Innovation, the National Sciences and Engineering Research Council of Canada – NSERC (grant RGPIN-2014-03606, ID), the Manitoba Research and Innovation Fund, the University of Manitoba, Aarhus University, the Greenland Institute of Natural Resources, and the EU project NACLIM (grant agreement 308299, BR). P.G.M. was supported by the NSERC grants RGPIN 227438-09, RGPIN 04357, and RGPCC 433898. The model experiment was performed on Compute Canada infrastructure. The NEMO model is available through the NEMO website (http://www.nemo-ocean.eu/). The ANHA configuration and its output can be accessed at http://knossos.eas.ualberta.ca/xianmin/anha/index.html. We thank Ivali Lennert, Kunuk Lennert, and Egon Frandsen for technical assistance in the field. We also appreciate outstanding logistical support from the Station Nord Danish military personnel. This work is a contribution to the Arctic Science Partnership (ASP) and the ArcticNet Networks of Centres of Excellence programs. The mooring oceanographic data are available through the Polar Data Catalogue at https://www.polardata.ca, file identifier 12955_iso.

References

Aksenov, Y., Karcher, M., Proshutinsky, A., Gerdes, R., de Cuevas, B., Golubeva, E., et al. (2016). Arctic pathways of Pacific Water: Arctic Ocean Model Intercomparison experiments. *Journal of Geophysical Research: Oceans*, *121*, 27–59. https://doi.org/10.1002/2015JC011299

Alkire, M. B., Falkner, K. K., Boyd, T., & Macdonald, R. W. (2010). Sea-ice melt and meteoric water distributions in Baffin Bay and the Canadian Arctic archipelago. *Journal of Marine Research*, *68*(6), 767–798. https://doi.org/10.1357/002224010796673867

Amon, R. M. W., Budéus, G., & Meon, B. (2003). Dissolved organic carbon distribution and origin in the Nordic Seas: Exchanges with the Arctic Ocean and the North Atlantic. *Journal of Geophysical Research*, *108*(C7), 3221. https://doi.org/10.1029/2002JC001594

Bacon, S., Reverdin, G., Rigor, I. G., & Smith, H. M. (2002). A freshwater jet on the east Greenland shelf. *Journal of Geophysical Research*, *107*(C7), 3068. https://doi.org/10.1029/2001JC000935

Bamber, J. L., Westaway, R. M., Marzeion, B., & Wouters, B. (2018). The land ice contribution to sea level during the satellite era. *Environmental Research Letters*, *13*, 063008. https://doi.org/10.1088/1748-9326/aac2f0

Bendtsen, J., Mortensen, J., Lennert, K., Ehn, J. K., Boone, W., Galindo, V., et al. (2017). Sea ice breakup and marine melt of a retreating tidewater outlet glacier in northeast Greenland (81 N). *Scientific Reports*, *7*(1), 4941. https://doi.org/10.1038/s41598-017-05089-3

Bignami, F., & Hopkins, T. S. (1997). The water mass characteristics of the Northeast Water Polynya: Polar Sea data 1992–1993. *Journal of Marine Systems*, *10*, 139–156. https://doi.org/10.1016/S0924-7963(96)00079-6

Brugler, E. T., Pickart, R. S., Moore, G. W. K., Roberts, S., Weingartner, T. J., & Statscewich, H. (2014). Seasonal to interannual variability of the Pacific water boundary current in the Beaufort Sea. *Progress in Oceanography*, *127*, 1–20. https://doi.org/10.1016/j.pocean.2014.05.002

Budéus, G., Schneider, W., & Kattner, G. (1997). Distribution and exchange of water masses in the Northeast Water Polynya (Greenland Sea). *Journal of Marine Systems*, *10*, 139–156.

Carmack, E., & Chapman, D. C. (2003). Wind-driven shelf/basin exchange on an Arctic shelf: The joint roles of ice cover extent and shelfbreak bathymetry. *Geophysical Research Letters*, *30*(14), 1778. https://doi.org/10.1029/2003GL017526

Carmack, E. C., Yamamoto-Kawai, M., Haine, T. W. N., Bacon, S., Bluhm, B. A., Lique, C., et al. (2016). Freshwater and its role in the Arctic Marine System: Sources, disposition, storage, export, and physical and biogeochemical consequences in the Arctic and global oceans. *Journal of Geophysical Research: Biogeosciences*, *121*, 675–717. https://doi.org/10.1002/2015JG003140

Castro de la Guardia, L., Hu, X., & Myers, P. G. (2015). Potential positive feedback between Greenland ice sheet melt and Baffin Bay heat content on the west Greenland shelf. *Geophysical Research Letters*, *42*, 4922–4930. https://doi.org/10.1002/2015GL064626

Courtois, P., Hu, X., Pennelly, C., Spence, P., & Myers, P. G. (2017). Mixed layer depth calculation in deep convection regions in ocean numerical models. *Ocean Modelling*, *120*, 60–78. https://doi.org/10.1016/j.ocemod.2017.10.007

de Steur, L., Steele, M., Hansen, E., Morison, J., Polyakov, I., Olsen, S. M., et al. (2013). Hydrographic changes in the Lincoln Sea in the Arctic Ocean with focus on an upper ocean freshwater anomaly between 2007 and 2010. *Journal of Geophysical Research: Oceans*, *118*, 4699–4715. https://doi.org/10.1002/jgrc.20341

Dmitrenko, I. A., Kirillov, S. A., Forest, A., Gratton, Y., Volkov, D. L., Williams, W. J., et al. (2016). Shelfbreak current over the Canadian Beaufort Sea continental slope: Wind-driven events in January 2005. *Journal of Geophysical Research: Oceans*, *121*, 2447–2468. https://doi.org/10.1002/2015JC011514

Dmitrenko, I. A., Kirillov, S. A., Ivanov, V. V., Woodgate, R. A., Polyakov, I. V., Koldunov, N., et al. (2009). Seasonal modification of the Arctic Ocean intermediate water layer off the eastern Laptev Sea continental shelf break. *Journal of Geophysical Research*, *114*, C06010. https://doi.org/10.1029/2008JC005229

Dmitrenko, I. A., Kirillov, S. A., Myers, P. G., Forest, A., Tremblay, B., Lukovich, J. V., et al. (2018). Wind-forced depth-dependent currents over the eastern Beaufort Sea continental slope: Implications for Pacific water transport. *Elementa: Science of the Anthropocene*, *6*(1), 66. https://doi.org/10.1525/elementa.321

Dmitrenko, I. A., Kirillov, S. A., Rudels, B., Babb, D. G., Pedersen, L. T., Rysgaard, S., et al. (2017). Arctic Ocean outflow and glacier-ocean interaction modify water over the Wandel Sea shelf, northeast Greenland. *Ocean Science*, *13*, 1045–1060. https://doi.org/10.5194/os-13-1045-2017

Dmitrenko, I. A., Kirillov, S. A., Rysgaard, S., Barber, D. G., Babb, D. G., Pedersen, L. T., et al. (2015). Polynya impacts on water properties in a northeast Greenland fjord. *Estuarine, Coastal and Shelf Science*, *153*, 10–17. https://doi.org/10.1016/j.ecss.2014.11.027

Dmitrenko, I., Polyakov, I., Kirillov, S., Timokhov, L., Simmons, H., Ivanov, V., & Walsh, D. (2006). Seasonal variability of Atlantic water on the continental slope of the Laptev Sea during 2002–2004. *Earth and Planetary Science Letters*, *244*(3–4), 735–743. https://doi.org/10.1016/j.epsl.2006.01.067

Dodd, P. A., Heywood, K. J., Meredith, M. P., Naveira-Garabato, A. C., Marca, A. D., & Falkner, K. K. (2009). Sources and fate of freshwater exported in the east Greenland current. *Geophysical Research Letters*, *36*, L19608. https://doi.org/10.1029/2009GL039663

Dodd, P. A., Rabe, B., Hansen, E., Falck, E., Mackensen, A., Rohling, E., et al. (2012). The freshwater composition of the Fram Strait outflow derived from a decade of tracer measurements. *Journal of Geophysical Research*, *117*, C11005. https://doi.org/10.1029/2012JC008011

Falck, E. (2001). Contribution of waters of Atlantic and Pacific origin in the Northeast Water Polynya. *Polar Research*, *20*(2), 193–200. https://doi.org/10.1111/j.1751-8369.2001.tb00056.x

Falck, E., Kattner, G., & Budéus, G. (2005). Disappearance of Pacific Water in the northwestern Fram Strait. *Geophysical Research Letters*, *32*, L14619. https://doi.org/10.1029/2005GL023400

Fichefet, T., & Maqueda, M. A. M. (1997). Sensitivity of a global sea ice model to the treatment of ice thermodynamics and dynamics. *Journal of Geophysical Research*, *102*, 12,609–12,646. https://doi.org/10.1029/97JC00480

Granskog, M. A., Stedmon, C. A., Dodd, P. A., Amon, R. M. W., Pavlov, A. K., de Steur, L., & Hansen, E. (2012). Characteristics of colored dissolved organic matter (CDOM) in the Arctic outflow in the Fram Strait: Assessing the changes and fate of terrigenous CDOM in the Arctic Ocean. *Journal of Geophysical Research*, *117*, C12021. https://doi.org/10.1029/2012JC008075

Guay, C. K., Klinkhammer, G. P., Falkner, K. K., Benner, R., Coble, P. G., Whitledge, T. E., et al. (1999). High-resolution measurements of dissolved organic carbon in the Arctic Ocean by in situ fiber-optic spectrometry. *Geophysical Research Letters*, *26*(8), 1007–1010. https://doi.org/10.1029/1999GL900130

Guéguen, C., Guo, L., Yamamoto-Kawai, M., & Tanaka, N. (2007). Colored dissolved organic matter dynamics across the shelf-basin interface in the western Arctic Ocean. *Journal of Geophysical Research*, *112*, C05038. https://doi.org/10.1029/2006JC003584

Haine, T. W. N., Curry, B., Gerdes, R., Hansen, E., Karcher, M., Lee, C., et al. (2015). Arctic freshwater export: Status, mechanisms, and prospects. *Global and Planetary Change*, *125*, 13–35. https://doi.org/10.1016/j.gloplacha.2014.11.013

Holland, M. M., Finnis, J., Barrett, A. P., & Serreze, M. C. (2007). Projected changes in Arctic Ocean freshwater budgets. *Journal of Geophysical Research*, *112*, G04S55. https://doi.org/10.1029/2006JG000354

Hu, X., & Myers, P. G. (2013). A Lagrangian view of Pacific water inflow pathways in the Arctic Ocean during model spin-up. *Ocean Modelling*, *71*, 66–80. https://doi.org/10.1016/j.ocemod.2013.06.007

Hu, X., Sun, J., Chan, T. O., & Myers, P. G. (2018). Thermodynamic and dynamic ice thickness changes in the Canadian Arctic Archipelago in NEMO-LIM2 numerical simulations. *The Cryosphere*, *12*, 1233–1247. https://doi.org/10.5194/tc-12-1233-2018

Hunke, E. C., & Dukowicz, J. K. (1997). An elastic-viscous-plastic model for sea ice dynamics. *Journal of Physical Oceanography*, *27*, 1849–1867. https://doi.org/10.1175/1520-0485(1997)027<1849:AEVPMF>2.0.CO;2

Jones, E. P. (2001). Circulation in the Arctic Ocean. *Polar Research*, *20*(2), 139–146. https://doi.org/10.1111/j.1751-8369.2001.tb00049.x

Jones, E. P., & Anderson, L. G. (1986). On the origin of the chemical properties of the Arctic Ocean halocline. *Journal of Geophysical Research*, *91*, 10759–10767. https://doi.org/10.1029/JC091iC09p10759

Jones, E. P., Anderson, L. G., & Swift, J. H. (1998). Distribution of Atlantic and Pacific waters in the upper Arctic Ocean: Implications for circulation. *Geophysical Research Letters*, *25*, 765–768. https://doi.org/10.1029/98GL00464

Jones, E. P., Swift, J. H., Anderson, L. G., Lipizer, M., Civitarese, G., Falkner, K. K., et al. (2003). Tracing Pacific water in the North Atlantic Ocean. *Journal of Geophysical Research*, *108*(C4), 3116. https://doi.org/10.1029/2001JC001141

Kalnay, E., Kanamitsu, M., Kistler, R., Collins, W., Deaven, D., Gandin, L., et al. (1996). The NCEP/NCAR 40-year reanalysis project. *Bulletin of the American Meteorological Society*, *77*, 437–471. https://doi.org/10.1175/1520-0477(1996)077<0437:TNYRP>2.0.CO;2

Kirillov, S., Dmitrenko, I., Rysgaard, S., Babb, D., Ehn, J., Bendtsen, J., et al. (2018). The inferred formation of a sub-ice platelet layer below the multiyear landfast sea ice in the Wandel Sea (NE Greenland) induced by meltwater drainage. *Journal of Geophysical Research: Oceans*, *123*, 3489–3506. https://doi.org/10.1029/2017JC013672

Kirillov, S., Dmitrenko, I., Rysgaard, S., Babb, D., Toudal Pedersen, L., Ehn, J., et al. (2017). Storm-induced water dynamics and thermohaline structure at the tidewater Flade Isblink Glacier outlet to the Wandel Sea (NE Greenland). *Ocean Science*, *13*, 947–959. https://doi.org/10.5194/os-13-947-2017

Limoges, A., Ribeiro, S., Weckström, K., Heikkilä, M., Zamelczyk, K., Andersen, T. J., et al. (2018). Linking the modern distribution of biogenic proxies in high Arctic Greenland shelf sediments to sea ice, primary production, and Arctic-Atlantic inflow. *Journal of Geophysical Research: Biogeosciences*, *123*, 760–786. https://doi.org/10.1002/2017JG003840

Lique, C., & Steele, M. (2012). Where can we find a seasonal cycle of the Atlantic water temperature within the Arctic Basin? *Journal of Geophysical Research*, *117*, C03026. https://doi.org/10.1029/2011JC007612

Madec, G. and the NEMO team: NEMO ocean engine (2008). Note du Pôle de modélisation. Institut Pierre-Simon Laplace (IPSL), France, 27, ISSN No 1288–1619.

Masina, S., Storto, A., Ferry, N., Valdivieso, M., Haines, K., Balmaseda, M., et al. (2017). An ensemble of eddypermitting global ocean reanalyses from the MyOcean project. *Climate Dynamics*, *49*, 813–841. https://doi.org/10.1007/s00382-015-2728-5

McLaughlin, F. A., Carmack, E. C., MacDonald, R. W., Melling, H., Swift, J. H., Wheeler, P. A., et al. (2004). The joint roles of Pacific and Atlantic-origin waters in the Canada Basin, 1997–1998. *Deep Sea Research Part I: Oceanographic Research Papers*, *51*, 107–128. https://doi.org/10.1016/j.dsr.2003.09.010

Morison, J., Kwok, R., Peralta-Ferriz, C., Alkire, M., Rigor, I., Andersen, R., & Steele, M. (2012). Changing Arctic Ocean freshwater pathways. *Nature*, *481*(7379), 66–70. https://doi.org/10.1038/nature10705

Nørgaard-Pedersen, N., Ribeiro, S., Mikkelsen, N., Limoges, A., & Seidenkrantz, M. S. (2016). Investigations of past climate and sea-ice variability in the fjord area by Station Nord, eastern North Greenland. *Geological Survey of Denmark and Greenland Bulletin*, *35*, 67–70.

Palmer, S. J., Shepherd, A., Sundal, A., Rinne, E., & Nienow, P. (2010). InSAR observations of ice elevation and velocity fluctuations at the Flade Isblink ice cap, eastern North Greenland. *Journal of Geophysical Research*, *115*, F04037. https://doi.org/10.1029/2010JF001686

Pickart, R. S., Weingartner, T. J., Pratt, L. J., Zimmermann, S., & Torres, D. J. (2005). Flow of winter-transformed Pacific water into the western Arctic. *Deep Sea Research, Part II*, *52*, 3175–3198. https://doi.org/10.1016/j.dsr2.2005.10.009

Prowse, T., Bring, A., Mård, J., & Carmack, E. (2015). Arctic freshwater synthesis: Introduction. *Journal of Geophysical Research: Biogeosciences*, *120*, 2121–2131. https://doi.org/10.1002/2015JG003127

Rabe, B., Karcher, M., Schauer, U., Toole, J. M., Krishfield, R. A., Pisarev, S., et al. (2011). An assessment of Arctic Ocean freshwater content changes from the 1990s to the 2006–2008 period. *Deep Sea Research Part I: Oceanographic Research Papers*, *58*(2), 173–185. https://doi.org/10.1016/j.dsr.2010.12.002

Rinne, E. J., Shepherd, A., Palmer, S., van den Broeke, M. R., Muir, A., Ettema, J., & Wingham, D. (2011). On the recent elevation changes at the Flade Isblink ice cap, northern Greenland. *Journal of Geophysical Research*, *116*, F03024. https://doi.org/10.1029/2011JF001972

Rodell, M., Famiglietti, S., Wiese, D. N., Reager, J. T., Beaudoing, H. K., Landerer, F. W., & Lo, M.-H. (2018). Emerging trends in global freshwater availability. *Nature*, *557*, 651–659. https://doi.org/10.1038/s41586-018-0123-1

Serreze, M. C., Barrett, A. P., Slater, A. G., Woodgate, R. A., Aagaard, K., Lammers, R. B., et al. (2006). The large-scale freshwater cycle of the Arctic. *Journal of Geophysical Research*, *111*, C11010. https://doi.org/10.1029/2005JC003424

Shimada, K., Itoh, M., Nishino, S., McLaughlin, F., Carmack, E., & Proshutinsky, A. (2005). Halocline structure in the Canada Basin of the Arctic Ocean. *Geophysical Research Letters*, *32*, L03605. https://doi.org/10.1029/2004GL021358

Shroyer, E. L., & Pickart, R. S. (2018). Pathways, timing, and evolution of Pacific Winter Water through Barrow Canyon. *Deep-Sea Research Part II: Topical Studies in Oceanography*. https://doi.org/10.1016/j.dsr2.2018.05.004

Smith, G. C., Roy, F., Mann, P., Dupont, F., Brasnett, B., Lemieux, J.-F., et al. (2014). A new atmospheric dataset for forcing ice–ocean models: Evaluation of reforecasts using the Canadian global deterministic prediction system. *Quarterly Journal of the Royal Meteorological Society*, *140*, 881–894. https://doi.org/10.1002/qj.2194

Stedmon, C. A., Amon, R. M. W., Rinehart, A. J., & Walker, S. A. (2011). The supply and characteristics of colored dissolved organic matter (CDOM) in the Arctic Ocean: Pan Arctic trends and differences. *Marine Chemistry*, *124*(1–4), 108–118. https://doi.org/10.1016/j.marchem.2010.12.007

Stedmon, C. A., Granskog, M. A., & Dodd, P. A. (2015). An approach to estimate the freshwater contribution from glacial melt and precipitation in east Greenland shelf waters using colored dissolved organic matter (CDOM). *Journal of Geophysical Research: Oceans*, *120*, 1107–1117. https://doi.org/10.1002/2014JC010501

Steele, M., Morison, J., Ermold, W., Rigor, I., Ortmeyer, M., & Shimada, K. (2004). Circulation of summer Pacific halocline water in the Arctic Ocean. *Journal of Geophysical Research*, *109*, C02027. https://doi.org/10.1029/2003JC002009

Sutherland, D. A., & Pickart, R. S. (2008). The east Greenland coastal current: Structure, variability, and forcing. *Progress in Oceanography*, *78*(1), 58–77. https://doi.org/10.1016/j.pocean.2007.09.006

Sutherland, D. A., Pickart, R. S., Peter Jones, E., Azetsu-Scott, K., Jane Eert, A., & Ólafsson, J. (2009). Freshwater composition of the waters off southeast Greenland and their link to the Arctic Ocean. *Journal of Geophysical Research*, *114*, C05020. https://doi.org/10.1029/2008JC004808

Timmermans, M.-L., Marshall, J., Proshutinsky, A., & Scott, J. (2017). Seasonally derived components of the Canada Basin halocline. *Geophysical Research Letters*, *44*, 5008–5015. https://doi.org/10.1002/2017GL073042

Tremblay, J. E., Bélanger, S., Barber, D. G., Asplin, M., Martin, J., Darnis, G., et al. (2011). Climate forcing multiplies biological productivity in the coastal Arctic Ocean. *Geophysical Research Letters*, *38*, L18604. https://doi.org/10.1029/2011GLo48825

von Appen, W.-J., & Pickart, R. S. (2012). Two configurations of the Western Arctic Shelfbreak current in summer. *Journal of Physical Oceanography*, *42*, 329–351. https://doi.org/10.1175/JPO-D-11-026.1

Watanabe, J. (2013). Linkages among halocline variability, shelf-basin interaction, and wind regimes in the Beaufort Sea demonstrated in pan-Arctic Ocean modeling framework. *Ocean Modelling*, *71*, 43–53. https://doi.org/10.1016/j.ocemod.2012.12.010

Weingartner, T., Cavalieri, D., Aagaard, K., & Sasaki, Y. (1998). Circulation, dense water formation, and outflow on the northeast Chukchi shelf. *Journal of Geophysical Research*, *103*(C4), 7647–7661. https://doi.org/10.1029/98JC00374

Woodgate, R. (2013). Arctic Ocean circulation: Going around at the top of the world. *Nature Education Knowledge*, *4*(8), 8.

Woodgate, R. A., Aagaard, K., & Weingartner, T. J. (2005). Monthly temperature, salinity, and transport variability of the Bering Strait through flow. *Geophysical Research Letters*, *32*, L04601. https://doi.org/10.1029/2004GL021880

Woodgate, R. A., Weingartner, T. J., & Lindsay, R. (2012). Observed increases in Bering Strait oceanic fluxes from the Pacific to the Arctic from 2001 to 2011 and their impacts on the Arctic Ocean water column. *Geophysical Research Letters*, *39*, L24603. https://doi.org/10.1029/2012GL054092

Zhong, W., Steele, M., Zhang, J., & Zhao, J. (2018). Greater Role of Geostrophic Currents in Ekman Dynamics in the Western Arctic Ocean as a Mechanism for Beaufort Gyre Stabilization. *Journal of Geophysical Research: Oceans*, *123*(1), 149–165. https://doi.org/10.1002/2017JC013282